



HAL
open science

FEA of oblique impact tests on a motorcycle helmet

N.J. Mills, S. Wilkes, S. Derler, A. Flisch

► **To cite this version:**

N.J. Mills, S. Wilkes, S. Derler, A. Flisch. FEA of oblique impact tests on a motorcycle helmet. International Journal of Impact Engineering, 2009, 36 (7), pp.913. 10.1016/j.ijimpeng.2008.12.011 . hal-00574810

HAL Id: hal-00574810

<https://hal.science/hal-00574810v1>

Submitted on 9 Mar 2011

HAL is a multi-disciplinary open access archive for the deposit and dissemination of scientific research documents, whether they are published or not. The documents may come from teaching and research institutions in France or abroad, or from public or private research centers.

L'archive ouverte pluridisciplinaire **HAL**, est destinée au dépôt et à la diffusion de documents scientifiques de niveau recherche, publiés ou non, émanant des établissements d'enseignement et de recherche français ou étrangers, des laboratoires publics ou privés.

Accepted Manuscript



Title: FEA of oblique impact tests on a motorcycle helmet

Authors: N.J. Mills, S. Wilkes, Field Archaeology, S. Derler, A. Flisch, St Gallen Switzerland

PII: S0734-743X(08)00330-8

DOI: [10.1016/j.ijimpeng.2008.12.011](https://doi.org/10.1016/j.ijimpeng.2008.12.011)

Reference: IE 1741

To appear in: *International Journal of Impact Engineering*

Received Date:

Revised Date:

Accepted Date:

Please cite this article as: Mills NJ, Wilkes S, Archaeology F, Derler S, Flisch A, Switzerland SG. FEA of oblique impact tests on a motorcycle helmet, *International Journal of Impact Engineering* (2009), doi: [10.1016/j.ijimpeng.2008.12.011](https://doi.org/10.1016/j.ijimpeng.2008.12.011)

This is a PDF file of an unedited manuscript that has been accepted for publication. As a service to our customers we are providing this early version of the manuscript. The manuscript will undergo copyediting, typesetting, and review of the resulting proof before it is published in its final form. Please note that during the production process errors may be discovered which could affect the content, and all legal disclaimers that apply to the journal pertain.

FEA of oblique impact tests on a motorcycle helmet

N.J. Mills, Metallurgy and Materials, University of Birmingham, UK

S. Wilkes, Field Archaeology, University of Birmingham, UK.

S. Derler & A. Flisch, EMPA, St Gallen, Switzerland.

ABSTRACT

In accidents, motorcycle riders full-face helmets often make oblique impacts with road surfaces. Finite Element Analysis was used to predict the rotational and linear acceleration of a Hybrid II headform, representing a motorcyclist's head, in such impacts, considering the effects of friction at the head/helmet and helmet/road interfaces. Simulations of the oblique impact test in British Standard BS 6658 were validated by comparison with published data. This showed that COST 327 experimental data was largely determined by the friction coefficient (0.55) between the helmet shell and abrasive paper, and hardly affected by that between the head and helmet. Slip was predicted at the shell/paper interface throughout the impact, due to the high angular inertia of the helmet, and the normal force remaining below 3.5 kN. Simulations of more severe motorcycle helmet impacts explored the effects of impact site and direction, impact velocity components, helmet fit and the scalp. In these impacts, the higher velocity component normal to the road caused high frictional forces on the helmet shell, eventually causing it to roll on the road. The peak headform rotational accelerations, at some impact sites, were potentially injurious. The most effective method of reducing head rotational acceleration could be a reduction in the linear acceleration limit of the helmet standards.

Keywords: motorcycle helmet, oblique impact, Finite Element Analysis

INTRODUCTION

Motorcycle helmets nearly always impact the road surface obliquely [1], rather than perpendicularly, causing both linear and rotational acceleration of the head (these terms refer, throughout the paper, to the accelerations of the head's centre of mass). Excessive head rotational acceleration causes brain damage to animals [2]. Research [3, 4] suggests that the rotational acceleration must exceed circa 10 krad s^{-2} in the mid-sagittal plane (dividing

symmetrical left and right halves) to cause subdural haematomas in humans. However, in motorcycle helmet test standards [5, 6], the majority of test impacts are perpendicular to the surface of fixed anvils, and the peak headform linear acceleration is used as a pass/fail criterion. This implies that the acceleration is unaffected by the head velocity component tangential to the anvil surface, and that peak linear acceleration determines head injury severity. A review of motorcycle helmet effectiveness [7] showed that wearing a helmet reduced the risk of head injury by 72%, implying that helmet design was effective but not ideal. Attempts have been made to associate particular motorcyclists' head injuries with head translation and head rotation [8], but headform rotational acceleration is not measured in helmet standards.

A review (chapter 16 of [9]) concluded that Finite Element Analysis (FEA) of direct impacts, on helmets containing a near-uniform thickness of expanded polystyrene bead foam (EPS) liner, was reasonably successful. However, for at least 10 years, nearly all helmets have had softer structures in the crown region (holes or grooves in a single density liner, or a lower density EPS or other foam as a crown insert), a feature not considered in the FEA. Helmet shells are stiffest when loaded at the crown [10], since that site has a doubly-convex curvature and is distant from any free edges. The softer liner in the crown region compensates for the high shell stiffness, and attempts to make the helmet impact response independent of site. The earlier FEA assumed that the EPS liner was bonded to the shell, whereas in practise it is either unbonded or only bonded in a small area at the crown. Glass fibre reinforced polyester resin (GRP) is used for many helmet shells, but its elastic properties depend on the processing conditions. Researchers often used GRP Young's moduli measured using flat test coupons, rather than values deduced from tests on helmet shells; Kostoupoulos et al. [11] used an in-plane Young's modulus of 19.7 GPa for a 2 mm thick prototype GRP shell. Aiello et al [12], who simulated direct impacts on a full-face Dainese helmet with a mixed-fibre composite shell, used an in-plane Young's modulus of 24 MPa at 50 °C. The consequent overestimation of the shell bending stiffness increased its load spreading to the EPS liner (the volume undergoing a high compressive strain), and hence gave erroneous predictions of helmet performance. The FEA often simplified the helmets, omitting chin-straps and foam inside the chin bar (which affect helmet rotation on the head), and the headform scalp.

No FEA has been reported of motorcycle helmet oblique impacts. In this multi-body problem, slip or rolling is possible at both the helmet inner and outer surfaces. The non-spherical head does not exactly fit the helmet liner, and the helmet liner does not exactly fit the helmet shell.

Prototype helmets [13], [14] aim respectively to reduce the friction inside and outside the helmet shell, by introducing easy-shear layers. The developers argued that this would reduce head rotational accelerations. However, such claims need to be demonstrated either experimentally, or by FEA.

There are few reports of headform acceleration measurements during motorcycle helmet oblique impacts; Aldman et al. [15] dropped a complete, helmet-wearing dummy onto a 1 metre diameter rotating road surface. The vertical velocity was 5.2 ms^{-1} (typical of free fall from a riding head height of about 1.5 metres) while the horizontal velocity component was 8.3 ms^{-1} . The peak headform angular accelerations ranged from 7 to 14 krad s^{-2} , with higher values on an abrasive paper surface than on a surface of rounded stones. The peak headform linear accelerations ranged from 105 to 180 g, the same as for vertical drops at the same velocity onto a road surface.

The oblique impact test rig of BS 6658 [5] uses a flat steel anvil, covered with a sheet of close-coated alumina abrasive paper, inclined at 15° to the vertical. The headform and helmet have a vertical velocity of 10 ms^{-1} at impact; the velocity components normal and tangential to the anvil surface are respectively $V_N = 2.59 \text{ ms}^{-1}$ and $V_T = 9.66 \text{ ms}^{-1}$. Although V_T may be representative of some motorcycle crashes, V_N is much smaller than for typical falls. The test was introduced in 1985 to render obsolete meetings of expert assessors, who determined whether helmet geometries met the requirements of the previous standard BS 2495 [16]. It was not intended to simulate typical crashes, and headform accelerations were not measured. The COST 327 project [17] used this test rig for oblique impacts on the sides of four types of motorcycle helmets with thermoplastic or GRP shells. The Hybrid II headform used had a plasticized PVC 'scalp' but no hair. Its 570 mm circumference was just smaller than the nominal 580 mm circumference of the helmets tested, so it was a good fit to the helmet liners. As the tests were limited to one site and direction, the range of peak headform rotational accelerations (2.4 to 8.5 krad s^{-2}), for impact velocities from 6 to 12 m s^{-1} , will be less than that in real crashes. The friction coefficients for the helmet/abrasive paper interface ranged from 0.4 to 0.6.

FEA of bicycle helmet oblique impacts on a rough metal surface representing a road [18] revealed that the effective friction coefficient of the helmet was a function of the friction coefficients λ_R at the road/shell and λ_H at the head/liner interfaces. The results of oblique impact experiments [19], using an Ogle headform fitted with an acrylic wig, were replicated using $\lambda_R = 0.25$ and $\lambda_H = 0.2$. Bicycle helmets typically have much lower masses (0.3 kg) and

angular moments of inertia (9 to 13 kg cm²) than test headforms (typically 4 to 5 kg and circa 200 kg cm²). Typical full-face motorcycle helmets have roughly twice the mass and twice the angular inertia of open-face helmets; the masses ranged from 0.8 to 1.7 kg, and the angular moments of inertia from 88 to 250 kg cm² [20]. Their tangential impact velocity component in crashes is often much higher than those for bicycle helmets. Consequently the oblique impact responses of motorcycle and bicycle helmets are expected to differ.

One aim of the research was to estimate the peak head rotational accelerations when motorcyclists fall to the road. Comparison with estimated human tolerance levels [3, 4] and injury statistics should improve the understanding of head injury mechanisms. A second aim was establish the headform features and test conditions needed to realistically simulate crashes, hence to review the oblique impact tests in helmet standards. A third aim was to identify the factors that control the peak headform rotational acceleration in oblique impacts. The vertical velocity component largely determines the amount of EPS liner crushing, hence the peak headform linear acceleration [9]. Some sliding is expected to occur at the helmet shell-road and helmet-hair interfaces, so the friction coefficients should affect the peak tangential force on the head, which contributes to the head rotational acceleration. For bicycle helmets [18], the headform geometry relative to the helmet liner geometry (which changed as the foam crushed) affected the normal force distribution on the interface, hence influenced the peak headform rotational acceleration. This mechanism may also apply for motorcycle helmets.

FEA

Helmet geometry

A full-face motorcycle helmet with a GRP shell, that met EC Regulation 22 [6], was manufactured in 2001 by Mavet SRL, Campodoro, Italy. Its brand name was 'Dainese', its size 58 cm and its total mass 1395 g. The AGV full-face helmets (mass 1395 g, GRP shell) used in the COST 327 tests were no longer available, but a similar one was purchased on eBay in a nearly new condition; its geometry and foam densities were very similar to the Mavet helmet. Therefore the comparison of the FEA predictions with the COST test results is justified.

A medical X-ray computer tomography (CT) scanner at EMPA Dübendorf was used on the helmet after the chin-bar foam components were removed. The pixel size was 0.40 mm in the horizontal plane with 0.60 mm between slices. Such scans contain artefacts, especially from

metal components such as the steel ‘hanger plates’ to which the chin-straps are attached. A horizontal slice image (Figure 1) shows small gaps between the EPS liner and the GRP shell near the hanger plates. The liner is an interference fit in the shell, and is not bonded to it. The relative positions of the helmet components are visible in the CT scan. However, the image quality was inadequate for satisfactory extraction of the geometry for the two densities of EPS liner; their grey levels varied spatially (possibly due to the air channels between the beads) and overlapped with the grey levels of other components.

AMIRA software [21] was used in Birmingham University Archaeology Dept. to improve the image contrast. The extracted inner and outer surfaces of the helmet shell contained many small holes, artefacts of the image analysis, and included the steel hanger plate surfaces. Therefore Magics 12 software [22] was used to repair and simplify the shell geometry. Since the helmet shell was modelled in FEA by shell elements rather than by 3-D solid elements, only the shell inner surface was preserved. Much of the detail of the GRP weave on this surface was removed by localised smoothing and reducing the number of triangles in the .stl file to 6900. Figure 2 shows the helmet shell, as part of the complete FEA model.

Small ventilation holes in the helmet liner were filled (forehead ventilation uses complex-shaped holes, made by bonding an EPS insert to the main liner) before it and the chin bar foam components were laser scanned in Birmingham. Subsequently, the liner was cut vertically at one side with a band-saw, and the low density EPS crown moulding (which had been moulded through a hole in the crown of the main liner) was separated. The main part of the internal surface, where the two densities of EPS met, was part of an ellipsoid, with, at its top, radius of curvature 120 mm in the xy plane of Figure 3, and 100 mm in the yz plane. The vertical sides of the internal surface were part of a cylinder of elliptical cross-section, with half axes 94 and 78 mm. These surfaces were constructed in a CAD program Rhino [23], then used in ABAQUS [24] to separate the liner into two regions, which could be allocated different properties.

An initial chin-strap shape was created in ABAQUS CAE. A 25 mm wide strip, of radius of curvature 53 mm, was a close fit under the headform chin. It was linked on each side with two planar segments that passed around the cheek mouldings, and through the holes in the hanger plates. A preliminary ABAQUS run pulled the strap ends up through the hanger plates, until the strap conformed to the face and chin bar side mouldings. The shape of this deformed mesh was then imported into the main ABAQUS model; when used in the main model, it was initially stress free.

Helmet components and their masses

Figure 3 shows the helmet foam components on the headform. The hanger plate positions, and chin-strap passage around expanded polypropylene bead foam (EPP) cheek mouldings, are typical of helmets that pass the ‘retention (detaching) test’ of Regulation 22-05. The shell mass was 615 g after removing the chin-straps (50 g), hanger plates (26 g), plastic ventilation mouldings (23 g), visor mounts (21g), base and vision-opening trim (84 g). In Table 1 the ‘material mass’ is the product of the component volume and its density, while the ‘non-structural mass’ accounts for items rigidly attached to the component, such as adhesives, plastic clips joining the chin bar foams, and shell trim. Since the shell thickness modelled was 1.50 mm (see next section), 69 g of non-structural mass was added to correct the shell mass, while a further 107 g is added for trim and ventilation mouldings. The helmet would be tested without 105 g of visor and visor fixings, so it would have mass 1289 g. 208 g of flexible open-cell polyurethane (PU) foam, cloth and flexible PVC are not modelled, since they do not react to helmet acceleration on the 10 ms time scale of the impact (in subsidiary modelling, the effect of including the PU foam cheek pads, with material properties from the literature [25, 26], was a less than 1% change in the peak accelerations). For the same reason, the circa 3 mm thick layer, of cloth backed with PU foam, that fits inside the liner was not modelled. FEA showed that the model helmet had angular inertias 145, 145 and 135 kg cm² about ear-to-ear, crown-to-neck and nose-to-rear axes respectively ($1 \text{ kg cm}^2 = 10^{-4} \text{ kg m}^2$).

Helmet material properties

A form of reverse engineering was used to characterise the GRP helmet shell modulus. Sectioning the shell revealed a gel coat plus paint layer circa 40 µm thick, which was assumed to be insignificant for modelling purposes. There is thicker gel coat (polyester thermoset) near the sharp internal corners of the vision opening, which has Young’s modulus circa 3 GPa. The shell thickness was remarkably uniform, a result of pressure bag moulding; it varied from 1.3 to 1.5 mm over all but the chin bar and visor mount regions, but was 2.5 mm in the centre of the chin bar and circa 2 mm near the visor mounts. The shell density in the crown and chin bar areas was respectively 1830 ± 10 and 1670 kg m^{-3} . For a GRP shell of uniform density 1830 kg m^{-3} and area 0.1990 m^2 to have a mass of 615 g, its mean thickness would be 1.69 mm.

Experimental load-deflection relationships were measured quasi-statically for the three loading geometries shown in Figure 4. FEA was then performed for the same loading geometries; a GRP Young’s modulus $E_G = 8 \text{ GPa}$ and Poisson’s ratio 0.1 [27], with shell

thickness 1.50 mm, reproduced the experimental responses (Figure 5) within 5%. The peak force in the experimental crown-loading data occurred when ring shaped cracks appeared in the resin; data beyond this point should be ignored. There was a slightly larger error for crown loading; the stiffness there depends critically on the highly loaded area near the visor mounts. GRP of density 1830 kg m^{-3} would have an unrealistically high glass volume fraction $V_f = 0.48$, if the resin density was 1200 kg m^{-3} (the glass fibre density is 2540 kg m^{-3}). The resin is probably filled with a mineral powder to reduce shrinkage, hence its density exceeds 1200 kg m^{-3} . A more realistic $V_f = 0.3$, with $E_{\text{Glass}} = 80 \text{ GPa}$ and $E_{\text{resin}} = 3 \text{ GPa}$, leads to a fibre-direction Young's modulus in unidirectionally-reinforced GRP of $E_u = 26.1 \text{ GPa}$. The woven roving layers in the shell produced a material with near-isotropic in-plane Young's modulus of 8 GPa that is close to the expected [28] $3/8 E_u$, i.e. 9.8 GPa . Modelling of crown impacts of GRP shell helmets onto a 50 mm radius rigid hemisphere at 7.5 ms^{-1} [11] predicted a small region of delamination in the GRP; nevertheless 49% of the energy was stored elastically in the GRP compared with 8% dissipated by delamination. When GRP shell helmets are examined after BS 6658 test impacts on to flat anvils, no evidence of delamination is found. Therefore, as only flat surface impacts are considered here, failure mechanisms in the GRP were not modelled.

The 1.3 mm thick polyethyleneterephthalate PET fibre webbing chin-strap had material constants given in Table 2. These were obtained [18] by approximating the experimental tensile response of a length of chin-strap taken from a helmet.

Sections were cut from the EPS and EPP foam components with a band saw, removing the moulded surface, which is usually of a higher density. Their densities (Table 2) were measured with an electronic densimeter, using the Archimedes principle. The uniaxial-compressive response of low density closed-cell polymer foams on loading can be fitted with

$$\sigma_c = \sigma_{c0} + \frac{P_0 \varepsilon}{1 - \varepsilon - R} \quad (1)$$

where σ_c and ε are the engineering compressive stress and strain, P_0 the effective gas pressure in the cells, and R the foam relative density (the foam density divided by the density of solid polymer). Impact compression stress–strain parameters for the EPP [29] are given in Table 2. Stauffer [30] showed that the impact compressive stress, of EPS of densities 15 , 30 and 50 kg m^{-3} , was 20% higher for an impact velocity of 9 ms^{-1} , than it was in a compressive test at 75 mm s^{-1} . Therefore compression tests at a crosshead speed of 20 mm min^{-1} were performed on cubes of side approximately 25 mm cut from the EPS foams, and the data fitted with equation

(1). Figure 6 shows that this provides a good fit to the post-yield loading data. The σ_{C0} values from the straight line fit were increased by 20% before entering into Table 2. These values are consistent with literature impact data for the respective densities [31], [18] of EPS. The foam Poisson's ratios in Table 2 are values for the pre-yield response, measured at low strain rates with the equipment described in [9] chapter 5.

The limitations of the *crushable foam* material model in ABAQUS are discussed in chapter 6 of [9]; there is no hardening in simple shear, and the unloading after uniaxial compression is too sudden. It requires an input of the uniaxial compressive data, plus the ratios p_t / p_{C0} of respectively the initial yield pressures in hydrostatic tension and compression, and σ_{C0} / p_{C0} . $p_t / p_{C0} = 1.0$ and $\sigma_{C0} / p_{C0} = 1.933$ were used. The use of the model had been validated by comparing predictions with experimental data for compressive impact on truncated EPS pyramids [32], and oblique impacts on bicycle helmets [18]. Hence the limitations of the model do not cause significant errors for the type of deformation fields considered here.

Headform

A Hybrid II headform of width 160 mm was used at EMPA for helmet testing. The scanned shape of a 580 mm circumference headform had been used for bicycle helmet FEA [18]. Its 199 mm length equalled that of the 70th percentile adult male, but its 154 mm width was smaller than the 160 mm of 70% adult male. Therefore two versions of the headform were used; the original 'narrow' version and a 'broad' version with width stretched to 160 mm using Rhino CAD software.

The test headform had an approximately 10 mm thick plasticized PVC scalp stimulant outside the aluminium casting. The response of a similar headform scalp was measured [19] under plane strain compression conditions. The compressive stress vs. deflection graph up to a stress of 11 MPa was approximated by linear segments (Table 3) and used as the normal contact stiffness function of the head/helmet interface. This obviated the need to create and mesh the scalp geometry. The PVC scalp layer shear stiffness, measured in a slow shear test as $2.3 \times 10^8 \text{ Pa m}^{-1}$, was used as the interface 'elastic slip stiffness'. In [18] FEA predicted, for 200 mm drops onto a flat rigid table, peak linear headform accelerations at two sites that were within the range expected for biofidelic headforms.

The headform, with axes shown in Figure 3, had length 199 mm, breadth 154 mm, and the rotational moments of inertia of a test headform I_{xx} 199 kg cm², I_{yy} 237 kg cm² and I_{zz} 172 kg cm²[18]. In a wire frame projection onto the mid-sagittal plane at the start of a simulation (Figure 7), a circa 3 mm gap is seen between the liner interior and the headform, which is

filled in the real helmet with soft polyurethane foam. Hence there was no initial contact between the headform and the helmet liner. As there was no tension on the chin-strap at the start of the simulation, there was no initial compressive loading of the liner.

Contact conditions

Penalty contact algorithms were used for the interfaces; the default stiffness, normal to the interface, is ten times the underlying element stiffness.

At interfaces between the headform and the liner, cheek pads and chin bar foams, *elastic slip* (shear of the interface before slip occurs) simulated the shear of the scalp layer. The parameters for this and the normal stiffness function (Table 3) are given in the previous section. At the road/shell interface, a bi-linear contact stiffness had zero normal pressure at initial contact, 10 MPa at a 1 mm over-closure and 100 MPa at 2 mm over-closure. This reduced force oscillations to an acceptable level, while the < 1 mm peak over-closure was insignificant. Hard contact, with a friction coefficient of 0.5, prevented the liner outer surface sliding out of the shell inner surface. Elragi [33] reviewed conference papers and theses, and found 0.5 that the dynamic friction coefficient of low density EPS on itself exceeded 0.5. There is no published data for higher density EPS sliding on other substrates. The friction coefficient at the helmet shell/anvil interface was taken from the analysis of the COST 327 tests, in which the initial contact force was small and sliding was continuous; hence it is a dynamic friction coefficient.

Meshing

In preliminary FEA, the part meshes were seeded at 15, 10, 7 and 5 mm spacing; the final change caused less than 1% change in the predicted responses, so a 5 mm spacing was used subsequently. Verification of the liner mesh showed that the average shape factor (element volume/ optimal element volume) was 0.62 and the average aspect ratio was 1.8. 4-node linear tetrahedral elements C3D4 were used for the foams; the helmet liner had 251571, the central chin bar foam 19928, and the cheek pads 16632 elements. The shell had 21317 linear triangular shell elements S3R, the chin-strap 803 linear triangular membrane elements M3D3, while the headform and hanger plates had respectively 4222 and 235 linear rigid triangular elements R3D3. ABAQUS indicated the critical elements, which determine the time interval, were in the liner; the region around them was re-meshed, after faces were merged using virtual topology, to ensure the time interval exceeded 150 ns. This allows a reasonable CPU time of about 5 hours.

Impacts

The test rig coordinate system 2 axis (Figure 2) is normal to the anvil (road) surface, as is the impact velocity component V_N . The tangential velocity component V_T of the impact is along the 3 axis. The head orientations relative to the anvil are determined by a sequence of rotations, from an initial position with the crown touching the anvil and the face along the 3 axis (Table 4). The effect of the rotations 'Right 35 up at 45' are shown in Figure 2b. In the FEA headform acceleration components are determined in the 123 axes. Dynamic (explicit) ABAQUS was used for the 20 ms duration of impact, with the large deformation option.

COST 327 tests

The COST 327 motorcycle safety helmet project involved four European countries in accident surveys, the establishment of human injury tolerance, and the development of helmet test methods. Part of the last topic, carried out at EMPA, involved the development of oblique impact tests. A Hybrid II headform was equipped [17] with nine accelerometers (Endevco 7264B-2000), positioned on a mounting block in a 3-2-2-2 array, following the recommendations of Padgaonkar et al. [34]. The total mass, including mounting block and the accelerometers, was 4.77 kg. The accelerometer signals were fed to three voltage amplifiers (Endevco Model 136) and sampled at 100 kHz using two Nicolet BE490XE transient recorder boards.

The drop tests were performed onto an anvil inclined at 15° to the vertical, fitted to a steel block, fixed on a concrete block with a total weight of 1 tonne. The anvil, to the specifications of BS 6658, was equipped with a tri-axial Kistler type 9366AB force transducer, fixed on a mounting plate (230×300 mm), allowing the measurement of both normal and tangential force components. The grade 80 alumina coated paper, described in the introduction, was replaced after each impact. The accelerometer and force transducer signals, electronically filtered according to CFC600, were recorded for 25 ms. High speed video at 4500 frames/s was taken of one test. Data for an impact velocity of 10 m s^{-1} were used. The helmet (and headform) fall direction lay in its mid-sagittal plane, while its z axis (see Figure 3) was horizontal, and its x axis downwards.

FEA PREDICTIONS

Reproducing COST 327 tests

The ‘broad’ headform of mass 4.77 kg was used for these simulations. The impact velocity components normal and tangential to the anvil were $V_N = 2.59 \text{ m s}^{-1}$ and $V_T = 9.66 \text{ m s}^{-1}$. The experimental overall friction coefficient was used as the shell/road friction coefficient λ_R , while the unknown head/liner friction coefficient λ_H was varied (Table 5). The predicted peak normal F_N and tangential F_T reaction forces for the Mavet helmet were close to the respective experimental values, in spite of the helmets differing slightly in design and materials. However, as these predicted values were insensitive to λ_H , they did not allow the friction coefficient determination. The overall friction coefficients (Table 5), the slopes of straight-line fits to F_T vs. F_N data, are close to λ_R , and the correlation coefficients r are high, for all but $\lambda_H = 0.2$. The peak headform rotational acceleration increased almost in proportion with λ_H ; consequently a λ_H of 0.5 best replicated the COST 327 data. The tangential impulse, the time integral of F_T , increases slightly with λ_H , and the experimental impulses are consistent with $\lambda_H = 0.5$.

Figure 8 compares FEA predictions of F_T vs. F_N with experimental data. Both plots were nearly linear, implying that the shell slid on the anvil for the whole impact; this was confirmed by comparing (Figure 9) frames from the experimental movie with the FEA simulation at four times. After shell-to-anvil contact, the headform side approached the anvil, and both headform and helmet rotated. The oval shape of the shell base distorted significantly during the impact. Slip was observed at the head/liner interface in the FEA simulations for $\lambda_H = 0.2$, but not when $\lambda_H = 0.4$.

FEA predicted the force F_N had a small initial peak, then reduced somewhat as the shell partly rebounded from the anvil, before a main peak (Figure 10a). The magnitude and shape of the main peak agreed well with data for the AGV helmet. However the first peak is smaller than, and the main peak 2 ms later than, the experimental data. This time delay suggests the initial separation between the side of the model headform and the liner is 5 mm greater than in the experiments. Increasing the helmet shell mass locally near the impact site would increase the size of the first peak.

Figure 10b and 10c compare respectively the magnitudes of the total linear and total rotational accelerations with COST tests on the left and right sides of two helmets; the agreement is good, allowing for a 2 ms delay in the predicted responses.

The coupling of the helmet and headform masses can be assessed using plots of the reaction force magnitude vs. the linear acceleration magnitude (Figure 11). The initial portions of these graphs are non-linear, because the helmet shell accelerated before the liner impacted the

headform. The slope of the linear regression line can be used to evaluate the effective mass m_e of the helmet-headform combination. The 6.19 kg value for the COST 327 experiments exceeded the 5.36 kg for the FEA model (the respective correlation coefficients were 0.901 and 0.938). Since the total headform and helmet mass was 6.06 kg, the helmet and headform masses were well coupled in the experiments, probably due to tension in the chin-strap. In the FEA model no initial tension was applied to the chin-strap.

Figure 12 shows contours of the equivalent plastic true strain PEEQ on both surfaces of the liner, when the plastic zone size was maximal after 11 ms. The yielded zone is quite small and nearly circular on both surfaces. On the inner surface there is some yielding of the low density EPS insert, and the zone is limited by the rear ventilation groove.

In a $\lambda_H = 0.5$ simulation of a 257 g lighter helmet (without the non-structural mass of Table 1, so with moments of inertia 105, 109 and 100 kg cm²), the ratio F_T / F_N reduced after 15 ms, showing that the shell rolled on the anvil at the end of the contact. Therefore the helmet angular inertia must exceed a critical value to maintain slip at the shell/road interface. This critical value depends on the impact site, and the friction coefficients. In higher V_N simulations, which caused higher peak forces F_N , rolling was common and the plots were non-linear. Therefore, shell sliding only persisted on the abrasive anvil under COST 327 impact conditions because F_N remained relatively low and the full-face helmet angular inertia was high.

The correlation coefficients r between the rotational acceleration magnitude $|\ddot{\theta}|$ and the tangential force F_T were 0.86 and 0.88, for the AGV helmet data and the FEA simulation respectively, because the time dependences of the two variables differed. As with bicycle helmets [18], the line of action of the net force F_N from the large contact area does not pass through the headform centre of gravity, so F_N contributes to $\ddot{\theta}_1$. However, as the neck-to-crown axis rotational inertia of the helmet (143 kg cm²) was of similar magnitude to that of the headform (163 kg cm²), and the helmet could slip on the headform, the headform rotational acceleration could not be simply linked to the sum of these two contributions.

Simulation of typical oblique impacts in crashes

The validated FEA model was used to explore more severe impacts, simulating serious motorcycle crashes. A headform/liner friction coefficient of $\lambda_H = 0.2$, and a shell/road friction coefficient $\lambda_R = 0.4$, were found in bicycle helmet oblique impacts [17,18] using a wig on the

headform, and a roughened metal plate as the road surface. The headform mass of 4.26 kg represented the human head. The ‘narrow’ headform shape used is typical of an imperfect fit of motorcyclists’ heads to their helmets [35]; some have helmets that are tight at the sides and others at the front/rear. In the simulations, either one side of the chin-strap, or both sides for crown impacts, initially slackened as the EPS liner crushed. Later, for the frontal impacts, the chin-strap tightened after the helmet had rotated on the head, but the total chin-strap force was never high.

First, the impact site was varied, with a velocity V_N of 5 m s^{-1} representing a fall from a riding head height of about 1.5 m. The sites were chosen to induce rotations about the three headform axes. As the rider’s shoulder probably hits the road first for impacts below left/right 70° sites, a right 80° site was chosen, in place of the COST 327 impact site. The peak rotational headform accelerations, given in Tables 6 and 7, were smallest for the frontal 80° site because the contributions from F_T and F_N acted in opposite directions, as for bicycle helmets [18]. They were highest for the right 80° site, where the impact direction caused rotation about the headform crown-to-neck axis.

The maximum values of F_N and linear headform acceleration hardly changed as V_T increased from 5 to 10 m s^{-1} . However, $\dot{\theta}_i^{\max}$ increased somewhat with V_T , and exceeded the 10 krad s^{-2} level for the onset of diffuse axonal injury for the right 80° and the ‘right 45° up at 45° ’ sites. The value of F_T / F_N was affected by the impact site, and was only close to λ_R when $V_N = 10 \text{ ms}^{-1}$.

The minimum thickness of the EPS liner (Tables 6 and 7) was calculated from the closest distance between the headform and the road, allowing 1.5 mm for the shell thickness. At the crown and right 45° sites, this was more than half the original liner thickness, showing that the helmet had considerable protection in reserve. For impacts on the front of the helmet, the chin bar foam came into play; the predicted accelerations are for a headform with a rigid chin, rather than an articulated jaw.

Figure 13a and b compare the time dependence of the headform accelerations for the right 80° impact site and $V_N = 5 \text{ ms}^{-1}$, for three values of the tangential velocity V_T . As V_T increased, the linear acceleration peaks at 4.5 and 7.5 ms decreased in size slightly, while the acceleration was slightly greater at times $> 10 \text{ ms}$. In contrast, the initial rotational acceleration peak increased significantly in size and duration as V_T increased.

Second, a range of normal and tangential velocity components was used for the right 80° site (Table 7). The peak liner crush distance increased approximately in proportion to the velocity V_N . The peak linear headform acceleration is estimated to reach the 275 g limit when the minimum liner thickness is 15 mm; hence the liner density is higher than optimum for impacts onto flat surfaces. Even in direct impacts, there were significant rotational accelerations when $V_N \geq 5 \text{ ms}^{-1}$. In the oblique impacts, the peak rotational acceleration increases significantly with V_N , but hardly with V_T , while the variation of peak rotational acceleration (krad s^{-2}) with peak linear acceleration (g) could be described by

$$|\ddot{\theta}|_{\max} = 98.2|a|_{\max} - 1098 \quad (2)$$

with correlation coefficient $r = 0.986$. This relationship was similar to, but for greater a_{\max} values than, that reported in [17] for the COST 327 impact site, with coefficients $75.4 \text{ rad s}^{-1} \text{ g}^{-1}$ and $+500 \text{ rad s}^{-2}$, and $r = 0.91$.

In an individual high-velocity test (with parameters given by the 9th row in Table 7), the correlation coefficient between the tangential force F_T and $|\dot{\theta}|$ was only $r = 0.72$. However, the correlation between the maximum values, for a series of tests on nearly the same impact site, was reported [17] as $r = 0.97$, suggesting that the easily-measured $F_{T\max}$ could be used as a surrogate for the more-difficult-to-measure $|\dot{\theta}|_{\max}$. Figure 14 shows, for the FEA simulations in Tables 6 and 7, a good correlation for a single site ($r = 0.945$ for the right 80° site), but no overall pattern for a range of impact sites. For lateral impact sites, the reported [17] 3.17 slope of the best-fit line for a number of helmets is half the slope of 6.34 in Figure 14 for a slightly different impact site. Therefore measurements of $F_{T\max}$ are not surrogates for measurements of headform rotational acceleration.

The reported correlation [17] between the tangential impulse J_T (the time integral of F_T) and the peak headform rotational velocity was $r = 0.95$. When J_T values (Ns) from Tables 6 and 7 were plotted against V_T (m s^{-1}); the best-fit relationship was found to be

$$J_T = 1.52 V_T - 0.57 \quad (3)$$

with $r = 0.89$. The basis of this correlation is discussed later.

A shell/ road friction coefficient $\lambda_R = 0.2$ was used to simulate helmets with low-friction surface layers. However, this reduction in λ_R caused minor increases in the peak rotational accelerations at low V_N , and minor increases at high V_N (penultimate column in Table 7). For $V_N \geq 5 \text{ ms}^{-1}$, the main F_N peak, at about 5 ms into the impact, caused both large flat areas to form on the outsides of the shell and liner, and the liner inside to conform to the headform

surface over a similar area. The peak rotational acceleration occurred at this time. Therefore large geometry changes, caused by the high impact force F_N , influenced the peak rotational acceleration more than the value of λ_R .

When simulations were repeated for the wider COST 327 headform, the results, in the last 3 rows of Table 7, were similar to those for the narrow headform. Therefore headform fit does not greatly influence the peak headform accelerations.

DISCUSSION

The FEA modelling results will be discussed prior to the three research aims. A comparison, of compression tests on a complete shell with FEA of the same loading geometry, showed that the Young's modulus of the GRP in the Mavet helmet was relatively low. This is almost certainly true for other helmets, suggesting that the moduli used in [11] and [12] were probably too high. GRP fracture and delamination does not occur in the flat anvil impacts, so these phenomena were not modelled. However, to model impacts on kerbstone anvils, these phenomena should be included in the FEA, as in [12]. If FEA is to replace prototype testing, in developing helmet designs to pass EC Regulation 22 or BS 6658, it is vital to model all the main protective foam components; the cheek pad foam was loaded in impacts at the helmet side, and the chin bar centre foam was loaded in frontal impacts. However, it is reasonable to replace the thin layer of soft polyurethane foam, which lies between the EPS liner and the headform, by an air gap. FEA predictions were close to the data (F_N vs. time, F_T vs. F_N , and headform acceleration vs. time) from COST 327 oblique impact experiments [17]. Some minor differences remain, due to the non-availability of the tested helmet, and doubts about how tightly the headform was strapped into the helmet. The test conditions caused sliding to continue on the abrasive paper surface throughout contact. The good fit of the test headform to the helmet liner, the high friction at this interface, and the high helmet moment of inertia, were all factors that prevented sliding at the headform/helmet interface.

The BS 6658 oblique impact conditions, chosen by Glaister [36] to test helmet shell protrusions within the limitations of a drop tower, are less severe than the majority of injury-causing motorcycle crashes. Consequently, the COST 327 program did not evaluate protection against excessive rotational head acceleration in more-typical crashes. For rearwards impacts on the right 80° site, FEA predicted that, for typical $V_N \cong 5 \text{ ms}^{-1}$, $10 > V_T > 5 \text{ ms}^{-1}$ and $0.4 > \lambda_R > 0.2$, the peak headform rotational accelerations ranged from 14 to 15 krad s^{-2} . For some other helmet impact sites, the peak rotational accelerations for these

velocities (Table 6) are less than the estimated 10 krad s^{-2} for the onset of brain injury. A survey of motorcyclist head injuries [8] showed a quite high incidence of subdural haematomas, which can be caused by head rotation.

The headform used for rotational acceleration measurements in oblique impact tests should have a compliant scalp, and possibly a synthetic wig to simulate the hair, together with soft under-chin tissue. These features will lower the head/helmet friction coefficient compared with COST 327 experiments, hence allow helmet rotation. An impact velocity V_N in excess of 5 ms^{-1} would ensure that the normal component of impact force was typical of serious helmet impacts. Oblique impacts, of an instrumented headform wearing a helmet, could measure the friction coefficients of road surfaces; this is likely to be less than that for the abrasive paper in BS6658.

The FEA showed that the shell/road friction coefficient was not the only factor determining the peak headform rotational acceleration in typical crashes. The deformation of the helmet liner, and the distribution of normal stresses across its inner surface (which depends on the impact site and direction), also make substantial contributions. The latter factor is related to helmet fit; real heads typically fit helmet liners less well than headforms, on which some liners appear to be based. The results in Table 7 suggest that a low shell/road friction coefficient, proposed for improved helmets [13, 14], had little effect on the peak head rotational accelerations for lateral impact sites. Finan et al [37] found reductions in the acceleration, for a 'Front 45 down' site in the current nomenclature, when a low friction layer was added to the outer surface of an American football helmet, but an increase in acceleration for the equivalent 'rear 45 up' site. Hence the benefit, if any, of a low friction layer is site specific. Rolling on the shell/road interface caused the tangential force F_T to fall below that calculated from F_N and a single friction coefficient, and the helmet geometry changed in the impact region. Given these factors, and the complex nature of the load spreading from the shell to the foam components, FEA is the only method to predict the rotational acceleration experienced by motorcyclists' heads in typical crashes.

The abrasive-anvil oblique impact test in BS 6658 requires that the tangential force does not exceed 4 kN, while its time integral does not exceed 28 Ns. When the same equipment is used in Regulation 22-05, the impact velocity is reduced to 8.5 ms^{-1} , and the limiting parameters reduced to 3.5 kN and 25 Ns respectively. However the fourth from bottom row of Table 7 shows that the headform rotational acceleration could be 20 krad s^{-2} , for a helmet test that met the tangential force and force integral requirements, and the Regulation 22-05 requirement for a peak linear acceleration $< 275 \text{ g}$ in direct impacts with $V_N = 7.5 \text{ ms}^{-1}$. A simple model

(Figure 15) can be used to estimate the tangential impulse J_T from the moments of inertia of the helmet and headform, and explain why J_T correlates with V_T . Assuming that no slip occurs at the head/helmet interface, and that the helmet radius r remains constant during the contact (it typically varied from 138 mm to 118 mm in a COST type impact), the angular equivalent of the impulse – momentum equation for linear motion is

$$r J_T = I(\omega_2 - \omega_1) \quad (4)$$

The contribution of F_N to the headform angular velocity change is assumed to be zero. The initial angular velocity of the headform $\omega_1 = 0$ while the final value ω_2 is assumed to be that for rolling on the anvil. Ignoring any reduction in V_T during the impact (it typically drops from 9.66 to 6.9 ms^{-1}), $\omega_2 = V_H/r$ so

$$J_T \cong \frac{I V_T}{r^2} \quad (5)$$

Therefore, substituting the combined inertia of the Mavet helmet and headform $I_{zz} = 0.030 \text{ kg m}^2$ and $r = 0.13 \text{ m}$, the tangential impulse was estimated as 18 Ns, 12% higher than the values in Table 5 for the COST data and FEA simulation. For the same input data, equation (5) implies that the tangential impulse is proportional to 1.78 V_T , which is 17% greater than the relationship in equation (3). It seems unlikely that the 28 Ns limit, specified in BS6658, could be reached, because typical helmets have insufficient angular inertia. The purpose of the limit, in terms of head injury mechanisms, is unclear.

Consequently, a review of the standards may be in order. Equation (2) showed the peak headform rotational acceleration for the right 80° site was almost linearly related to the peak linear acceleration. A reduction in the latter, from 275 g towards 150 g, should proportionately reduce the peak rotational head acceleration. This could be achieved, without changing the helmet shell dimensions, by reducing the liner foam density, if the impact velocity into a kerbstone anvil was reduced from the current 7.5 m s^{-1} . This kerbstone impact test critically influences helmet design, because it causes a greater liner crushing distance than flat anvil impacts, hence it determines the liner density. Since the most common crash type is on flat surfaces, flat anvil impacts should have the greatest influence on helmet design. Consequently, a reduction in the kerbstone impact velocity should improve helmet protection for the majority of motorcyclists.

Conclusions

The peak head rotational acceleration, when motorcyclists fall obliquely to the road, was estimated by FEA to be the order of 15 krad s^{-2} for typical-velocity impacts at the side of the helmet; this level would probably cause rotational head injury.

To realistically simulate oblique helmet impacts in crashes, the test headform should have a compliant scalp, and soft under-chin tissue, rather than being entirely made of metal. The impact velocity component V_N normal to the test anvil should exceed 5 ms^{-1} to be typical of serious helmet impacts. The oblique impact tests currently in BS 6658 and EC Regulation 22 do not encourage the development of helmets that reduce peak rotational head accelerations, because the headforms lack the required features, V_N is too low, and the pass/fail criteria are not expressed in terms of rotational acceleration.

The peak headform rotational acceleration was shown to be a function of three main parameters: the impact velocity component normal to the road, the friction coefficient between the shell and road, and the impact site/direction.

It was relatively insensitive to the tangential component of impact velocity. The main reason why potentially-injurious peak rotational accelerations of 20 krad s^{-2} occurred, for some impact sites when $V_N = 7.5 \text{ ms}^{-1}$, was the high linear head acceleration permitted by helmet test standards.

Acknowledgements

Dr M. Lobb of the Birmingham University Field Archaeology Unit is thanked for performing laser scans of helmet foam components. Dr P. Brühwiler of EMPA kindly provided the Mavet helmet, and commented on the paper.

References

1. D. Otte, Technical demands on safety in the design of crash helmets: biomechanical analysis of real accident situations, (1991) SAE paper 912911.
2. T.A. Gennarelli, L.E. Thibault, J.H. Adams et al. Diffuse axonal injury and traumatic coma in the primate, *Ann. Neurol.* **12** (1982) 564-574.
3. B. Depreitere, C. van Lierde, J. vander Sloten et al., Mechanics of acute subdural haematomas resulting from bridging vein rupture, *J. Neurosurg.* **104** (2006) 950-956.
4. N. Yoganandan, F.A. Pintar et al., Biomechanical aspects of blunt and penetrating head injuries, IUTAM symposium Biomechanics of Impacts, Dublin, (2005) 173-184.
5. BS 6658:1985 Protective helmets for vehicle users, British Standards Institution, London.
6. UN ECE Regulation 22-05, Uniform provisions concerning the approval of protective helmets and their visors for drivers and passengers of motorcycles and mopeds, Geneva.
7. B. Liu, R. Ivers et al., Helmets for preventing injury in motorcycle riders, *Cochrane Library*, 2005 Issue 1.

8. M. Richter, D. Otte, U. Lehmann et al. Head injury mechanisms in helmet-protected motorcyclists, *J. Trauma*, **51** (2001) 949-958.
9. N.J. Mills, *Polymer Foams Handbook- Engineering and biomechanics applications and design guide*, Butterworth Heinemann, 2007.
10. A. Gilchrist & N.J. Mills, Impact deformation of ABS and GRP helmet shells, *Plast. Rubb. & Comp. Proc. & Appl.* **21** (1994) 151-160.
11. V. Kostopoulos, Y.P. Markopoulos, G. Gianonopoulos et al. FEA of impact damage response of composite motorcycle helmets, *Composites, Part B* **33** (2002) 97-107.
12. M. Aiello, U. Galvanetto & L. Iannucci, Numerical simulations of motorcycle helmet impact tests, *Int. J. Crashworthiness*, **12** (2007) 1-7.
13. P. Halldin, A. Gilchrist & N.J. Mills, A new oblique impact test for motorcycle helmets, *Int. J. Crashworthiness*, **6** (2001) 53-64.
14. K.D. Phillips (2004) European Patent EP1404189 Protective headgear and protective armour and a method of modifying protective headgear and protective armour.
15. B. Aldman, B. Lundell & L. Thorngren, Oblique impacts – a parametric study in crash helmets, IRCOBI (International Research Committee on Biokinetics of Impacts) conference, 1978, 129-141.
16. BS 2495:1977 Protective helmets for vehicle users (high protection), British Standards Institution, London.
17. COST 327: Motorcycle Safety Helmets (2001) Final report, Chapter 8. Directorate General for Energy and Transport, European Commission.
18. N.J. Mills & A. Gilchrist, Finite element analysis of bicycle helmet oblique impacts, *Int. J. Impact Engng.* **35** (2008) 1087-1101.
19. N.J. Mills & A. Gilchrist, Oblique impact testing of bicycle helmets, *Int. J. Impact Engng.* **35** (2008) 1075-1086.
20. N.J. Mills & R. Ward, The biomechanics of motorcycle helmet retention, IRCOBI Conference, 1985, 117-27.
21. AMIRA 4 software, Visage Imaging, Carlsbad, CA, USA.
22. MAGICS 12 software, Materialise NV, Leuven, Belgium.
23. Rhinoceros 3 software, Robert McNeel and associates, Seattle, USA.
24. ABAQUS 6.7, Hibbit, Karlsson and Sorensen Inc. Pawtucket, R.I., USA (2007).
25. N.J. Mills & A. Gilchrist, Modelling the indentation of low density polymer foams, *Cell. Polym.* **19** (2000) 389-412.
26. N.J. Mills, Finite Element models for the viscoelasticity of open-cell Polyurethane foam, *Cell. Polym.* **25** (2006) 293-316.
27. H.J. Lin, C.C. Tsai & J.S. Shie, Failure analysis of woven-roving composites with moulded in holes, *Comp. Sci. Tech.* **55** (1995) 231-9.
28. D. Hull, *Introduction to composite materials*, Cambridge Univ. Press, 1981.
29. N.J. Mills, Time dependence of the compressive response of polypropylene bead foam, *Cell. Polym.* **16** (1999) 194-215.
30. F. Stauffer, Sandwich-Strukturen für ein besseres Dämpfungsverhalten in Polystyrol-basierten Helmen, M.Sc thesis, ETH, Zürich, 2007.
31. H. Hazarika, Stress strain modelling for EPS geofom for large strain applications, *Geotext. & Geomemb.* **24** (2006) 79-90.
32. A. Gilchrist & N.J. Mills, Impact deformation of rigid polymeric foams: experiments and FEA modelling, *Int. J. Impact Engng.*, **25** (2001) 767-786.
33. A.F. Elragi at www.softoria.com/institute/geofom
34. A.J. Padgaonkar, K.W. Krieger & A.I. King, Measurement of angular acceleration of a rigid body using linear accelerometers, *J. Appl. Mech.* **42** (1975) 552-556.

35. A. Gilchrist, N.J. Mills & T. Khan, Survey of head, helmet and headform sizes related to motorcycle helmet design, *Ergonomics*, **31** (1988) 1395-1412.
36. D.H. Glaister & P. Mortimer, A test for the sliding resistance of protective helmets, RAF Institute of Aviation Medicine, Farnborough, Hants, Div. Record 28 (1982).
37. J.D. Finan, R.W. Nightingale & B.S Myers, The influence of reduced friction on head injury metrics in helmeted head impacts, *Traffic Inj. Prev.* **9** (2008) 483-488.

ACCEPTED MANUSCRIPT

Figure captions

Fig. 1. CT scan slice of Mavet helmet at level of the upper rivet on the hanger plate.

Fig. 2. Complete Mavet helmet in the impact positions a) right 80, reached by a 80° rotation about the 3 axis from a crown impact site, b) right 45 up at 45. The tangential velocity component, along the 3 axis, is towards the viewer.

Fig. 3. FEA model of Mavet helmet with its shell removed, revealing the foam components and chin-strap position. The $x y z$ axes of the headform are shown.

Fig. 4. Loading experiments for shell: crown (top), side, and chin.

Fig. 5. Comparison of experimental and FEA predictions for shell loading.

Fig. 6. Compressive loading and unloading data for the two densities of EPS from the Mavet helmet, plotted according to equation (1). The dotted lines are fits of the post-yield, loading response, for the range 0.1 to 5 of the strain parameter.

Fig. 7. Wire-frame view of initial position of helmet on headform; gaps between the liner inside (grey line) and the headform are visible.

Fig. 8. F_T versus F_N for oblique impacts with COST 327 conditions: FEA with $\lambda_R = 0.55$, $\lambda_H = 0.5$, compared with data for AGV helmet.

Fig. 9. Helmet and headform positions in COST 327 oblique impact test with $\lambda_R = 0.55$, $\lambda_H = 0.5$, compared with experiment at times a) 0.6 ms, b) 6 ms, c) 12 ms, d) 18 ms.

Fig. 10. FEA predictions (solid curve) for $\lambda_R = 0.55$, $\lambda_H = 0.5$ of oblique impact of Mavet helmet, with COST 327 data from four experiments shown as dotted curves, for AGV helmet: a) normal force, b) linear acceleration, c) rotational acceleration magnitude.

Fig. 11. Linear head acceleration vs. reaction force, comparing FEA with $\lambda_R = 0.55$, $\lambda_H = 0.4$ with COST data. The dotted lines are linear fits

Fig. 12. Contours of true plastic strain PEEQ in the liner after 11 ms of the COST simulation with $\lambda_R = 0.55$, $\lambda_H = 0.4$.

Fig. 13. Time dependence of a) peak linear acceleration and b) rotational acceleration, for three values of V_T (ms^{-1}), for a right 80° impact with $V_N = 5 \text{ ms}^{-1}$.

Fig. 14. Peak rotational head accelerations vs. peak tangential forces for data in tables 6 and 7. Correlation line and dots for right 80 site, triangles front 80, squares crown, crosses r45 site.

Fig. 15. Model for calculation of the tangential impulse.

Table 1. Helmet components in the FEA

component	Material mass (g)	Non-structural mass (g)	Total mass used in FEA (g)	Associated soft component ignored	mass (g)
Main liner	204	40	244	Cloth liner	63
Chin bar centre	13	29	42	Top, base cover	21
Cheek pad x 2	12.5 x 2	6 x 2	18.5 x 2	Cloth, PU foam	42 x 2
Chin strap	10		10	Covers, rings	40
Hanger plate x 2	13 x 2		13 x 2		
GRP shell	546	176	722		
TOTAL	824	257	1081		208

Table 2. Materials properties used in the FEA

material	Density (kg m^{-3})	Young's modulus E (MPa)	Poisson's ratio	Foam initial yield stress σ_{Co} (MPa)	effective gas pressure P_0 (MPa)
EPS crown insert	22	3.0	0.1	0.14	0.097
EPS main & chin	59	19	0.1	0.62	0.19
EPP cheek	70	20	0.1	0.76	0.27
GRP	1830	8000	0.1		
PET webbing	700	1000	0.2		

Table 3. Normal contact response of the PVC scalp simulant

pressure MPa	Over-closure mm
0	0
0.63	1
2.22	2
4.6	3
7.8	4
11.2	4.8

ACCEPTED MANUSCRIPT

Table 4. Rotations of the inverted head, facing the 3 axis, to reach the impact site

Site and <i>direction</i>	sequence of rotations
Crown <i>lateral</i>	90° about 2 axis
Front 80° <i>down</i>	80° about 1 axis
Right 80° <i>back</i>	80° about 3 axis
Right 45° <i>up at 45°</i>	45° about 3 axis, 45° about 2 axis
COST	180° about 2 axis, 90° about 3 axis, 15° about 1 axis

Table 5. Oblique impacts on a flat abrasive anvil, using COST 327 conditions, with $V_N = 2.59$ m s⁻¹ and $V_T = 9.66$ m s⁻¹

	Head λ_H	Road λ_R	overall λ	Correl r	F_N^{\max} (kN)	F_T^{\max} (kN)	Head a_{\max} (g)	Head $ \ddot{\theta} _{\max}$ (krad s ⁻²)	impulse I_T (Ns)
AGV			0.549	0.997	3.66	2.06	77	5.5	16.2
data.			± 0.016	± 0.001	± 0.22	± 0.08	± 4	± 0.4	± 0.7
FEA	0.2	0.55	0.525	0.985	3.80	2.06	93	1.8	13.9
FEA	0.4	0.55	0.549	0.9999	3.60	1.98	95	3.4	15.4
FEA	0.5	0.55	0.549	1.0000	3.49	1.92	97	5.2	15.9
FEA	0.7	0.55	0.550	0.9999	3.62	1.98	98	7.4	16.3

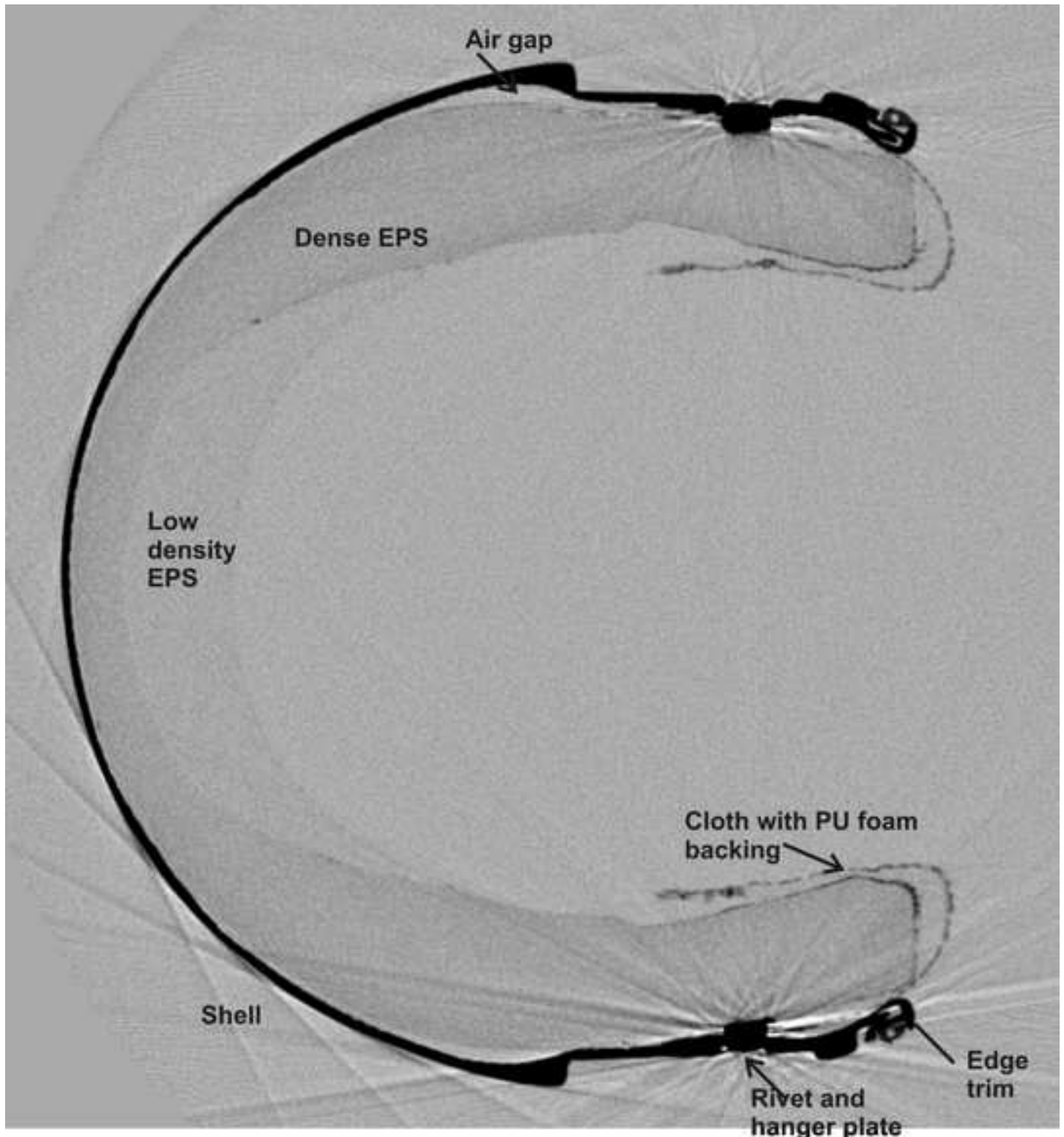
Table 6. Oblique impacts on flat surface, using $\lambda_R = 0.4$, $\lambda_H = 0.2$, and $V_N = 5.0 \text{ m s}^{-1}$, for a range of impact sites and tangential velocities.

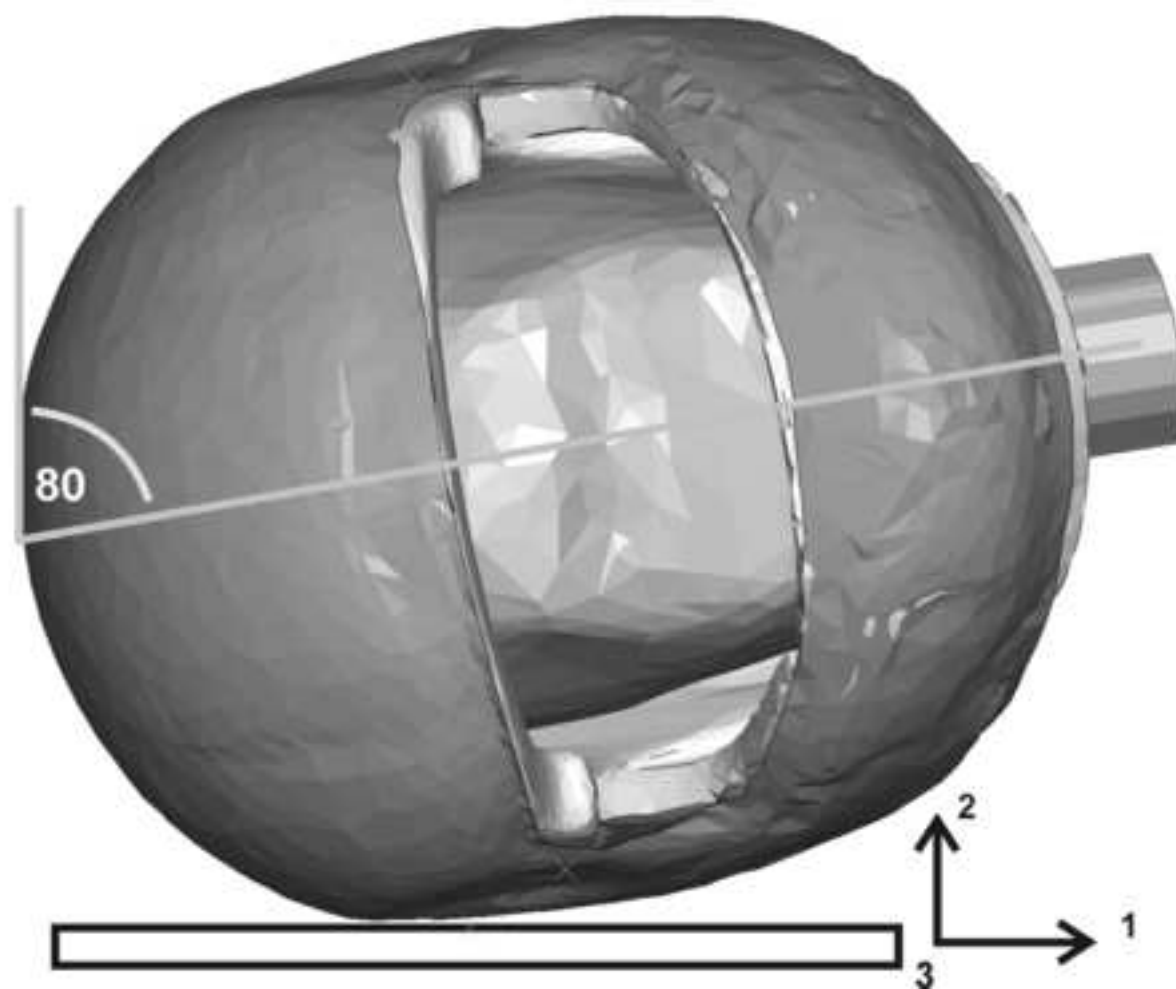
Impact site & direction	V_T (m s^{-1})	F_N^{\max} (kN)	F_T^{\max} (kN)	F_T/F_N (r)	liner x_{\min} (mm)	head a_{\max} (g)	head $\ddot{\theta}_1^{\max}$ (krad s^{-2})	head $\ddot{\theta}_2^{\max}$ (krad s^{-2})	head $\ddot{\theta}_3^{\max}$ (krad s^{-2})	head $ \ddot{\theta} _{\max}$ (krad s^{-2})	impulse J_T (Ns)
Front 80° down	0	7.08	0.99		16.6	135	2.7	0.6	-0.9	2.7	1.7
	5	6.63	2.58	0.425 (0.972)	18.8	154	3.4	0.8	0.6	3.4	14.9
	10	6.75	2.68	0.400 (1.000)	18.1	154	3.7	0.9	1.3	3.8	17.8
Crown lateral	0	5.50	0.50		22.7	138	0.8	-1.0	2.0	2.2	-0.2
	5	5.10	1.72	0.199 (0.709)	22.4	134	5.2	-2.1	1.6	5.7	8.4
	10	5.09	2.04	0.366 (0.948)	22.4	143	6.2	2.9	1.9	7.0	14.2
Right 45° Up at 45°	0	7.79	0.49		25.4	163	3.8	-2.5	2.6	4.7	-2.2
	5	8.04	2.04	0.217 (0.811)	26.7	170	10.7	-5.3	2.7	11.8	7.5
	10	8.14	3.23	0.350 (0.949)	26.7	170	12.3	-5.8	-2.9	12.7	13.7

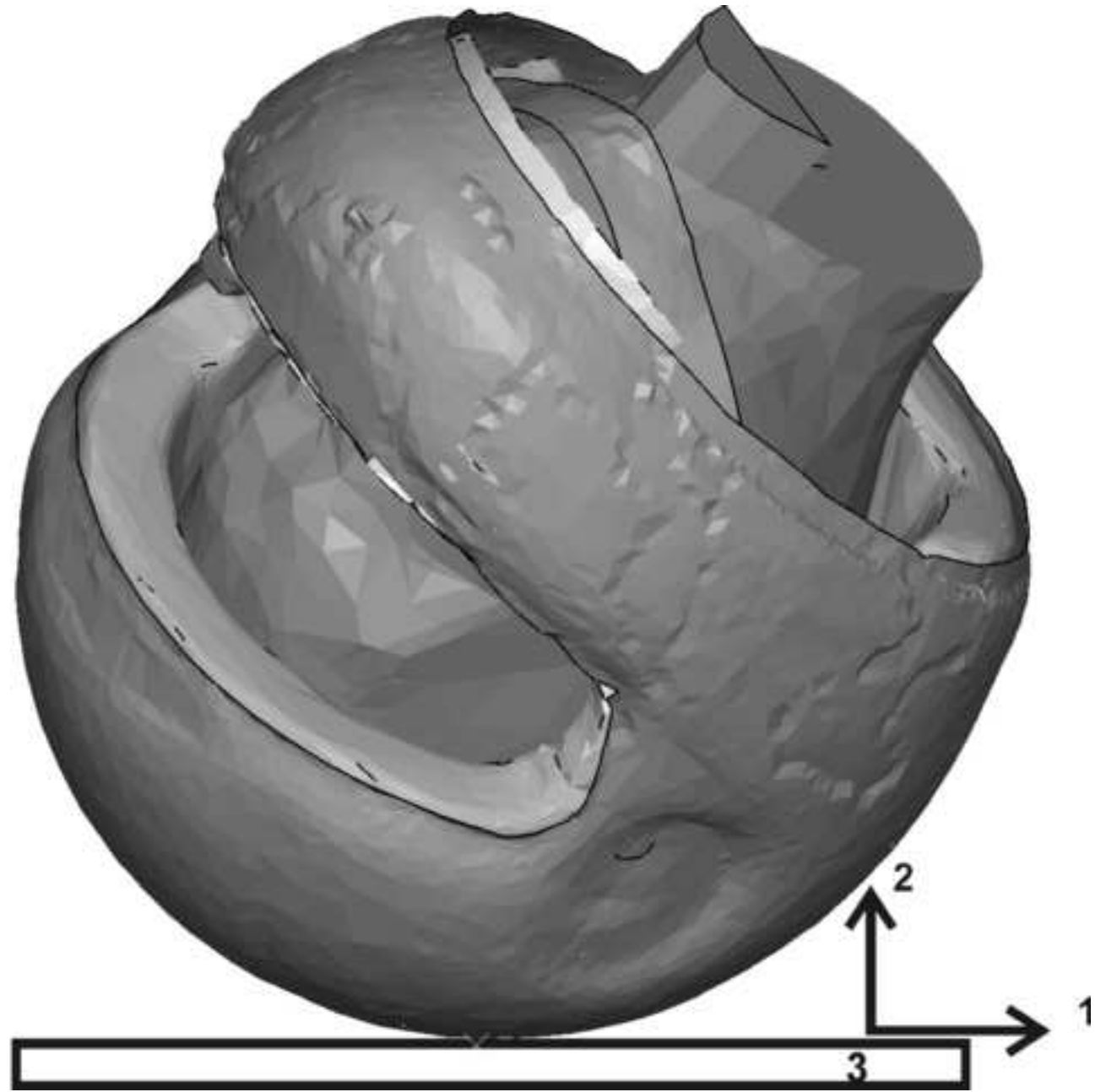
Table 7. Oblique impacts, rearwards on the right 80° site, on a flat surface with $\lambda_R = 0.4$, $\lambda_H = 0.2$, for a range of velocity components

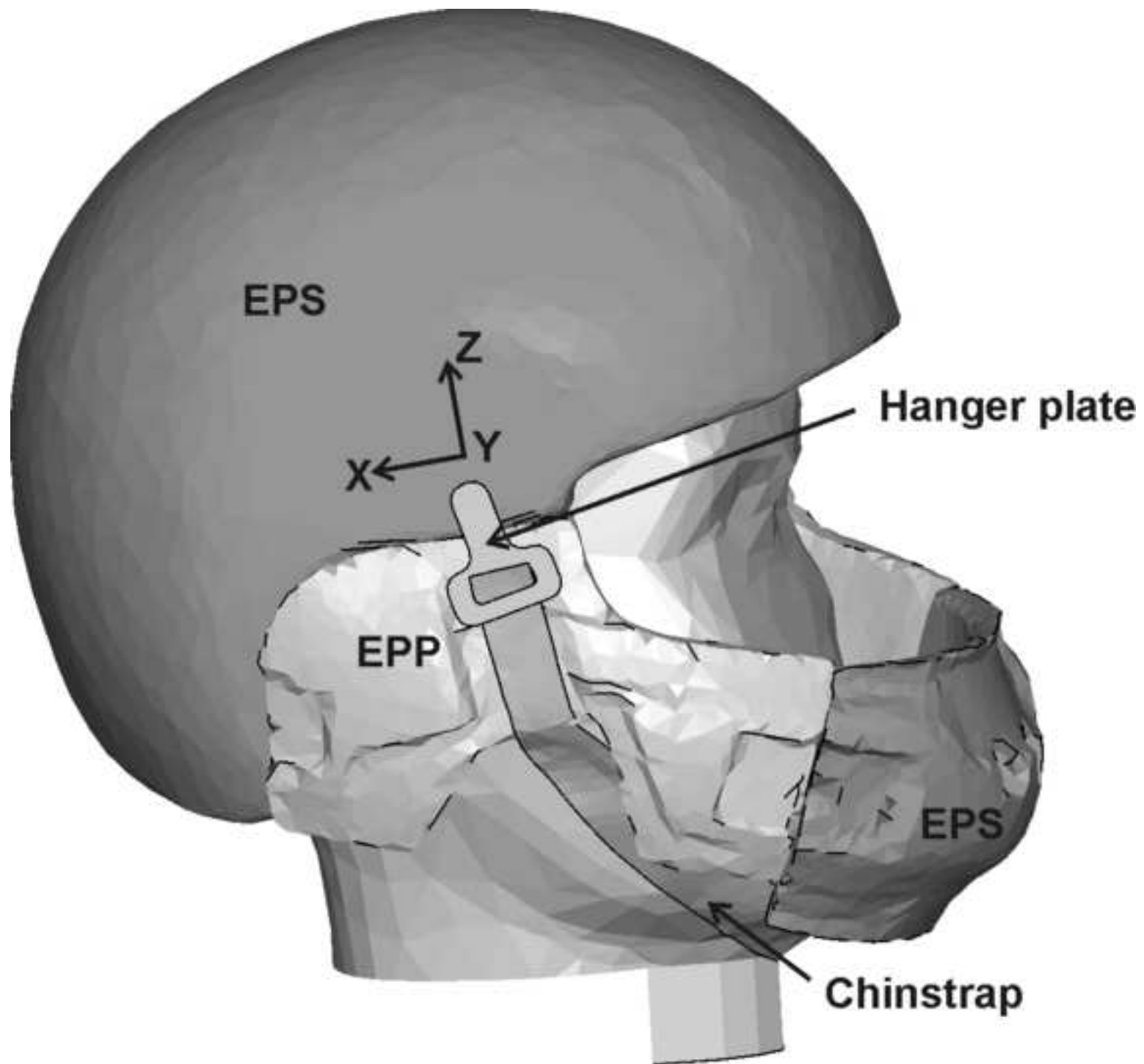
V_N (m s ⁻¹)	V_T (m s ⁻¹)	F_N^{\max} (kN)	F_T^{\max} (kN)	$F_T/F_N (r)$	liner x_{\min} (mm)	head a_{\max} (g)	head $\ddot{\theta}_1^{\max}$ (krad s ⁻²)	head $\ddot{\theta}_2^{\max}$ (krad s ⁻²)	head $\ddot{\theta}_3^{\max}$ (krad s ⁻²)	head $ \ddot{\theta} _{\max}$ (krad s ⁻²)	head $ \ddot{\theta} _{\max}$ $\lambda_R = 0.2$	impulse J_T (Ns)
2.5	0	2.62	0.30	-0.115 (0.50)	31.1	83	3.4	-0.6	3.1	3.9		-1.2
	5	2.54	0.94	0.360 (0.990)	31.5	68	4.3	1.4	2.9	4.8	5.3	6.3
	10	2.38	0.94	0.389 (0.999)	31.4	65	4.2	1.3	3.2	4.8	5.2	6.5
5.0	0	8.03	0.40	-0.084 (0.63)	25.3	155	7.7	-1.0	6.8	10.3		-2.8
	5	7.12	2.24	0.252 (0.829)	25.6	145	13.2	2.9	6.3	14.3	13.6	7.7
	10	6.73	2.43	0.354 (0.992)	25.3	140	12.5	2.9	6.2	13.8	13.6	13.3
7.5	0	11.95	0.53	-0.092 (0.65)	18.3	242	9.3	-1.6	8.1	12.2		-4.1
	5	11.10	2.77	0.14 (0.700)	18.7	226	18.1	3.0	8.3	19.5	19.0	8.2
	10	10.19	3.31	0.320(0.949)	18.5	208	18.4	3.7	8.0	19.9	19.8	18.5
2.5*	10	2.74	1.04	0.381 (0.999)	29.3	59	4.8	1.1	2.9	5.1		8.2
5.0*	10	7.15	2.39	0.338 (0.991)	22.6	131	11.9	2.3	5.7	13.0		
7.5*	10	10.11	3.06	0.310 (0.914)	14.7	205	16.6	3.6	7.0	18.1		

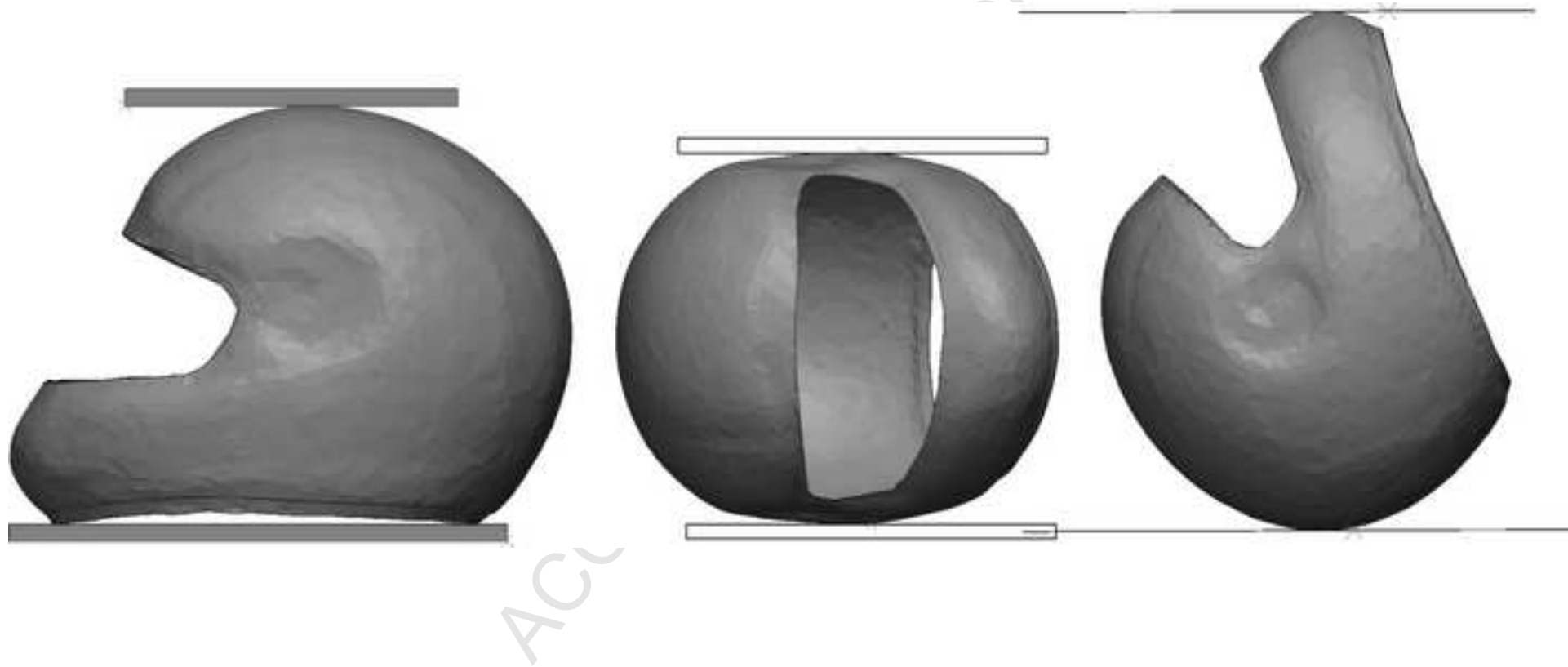
* using the wider headform of mass 4.77 kg





 V_N





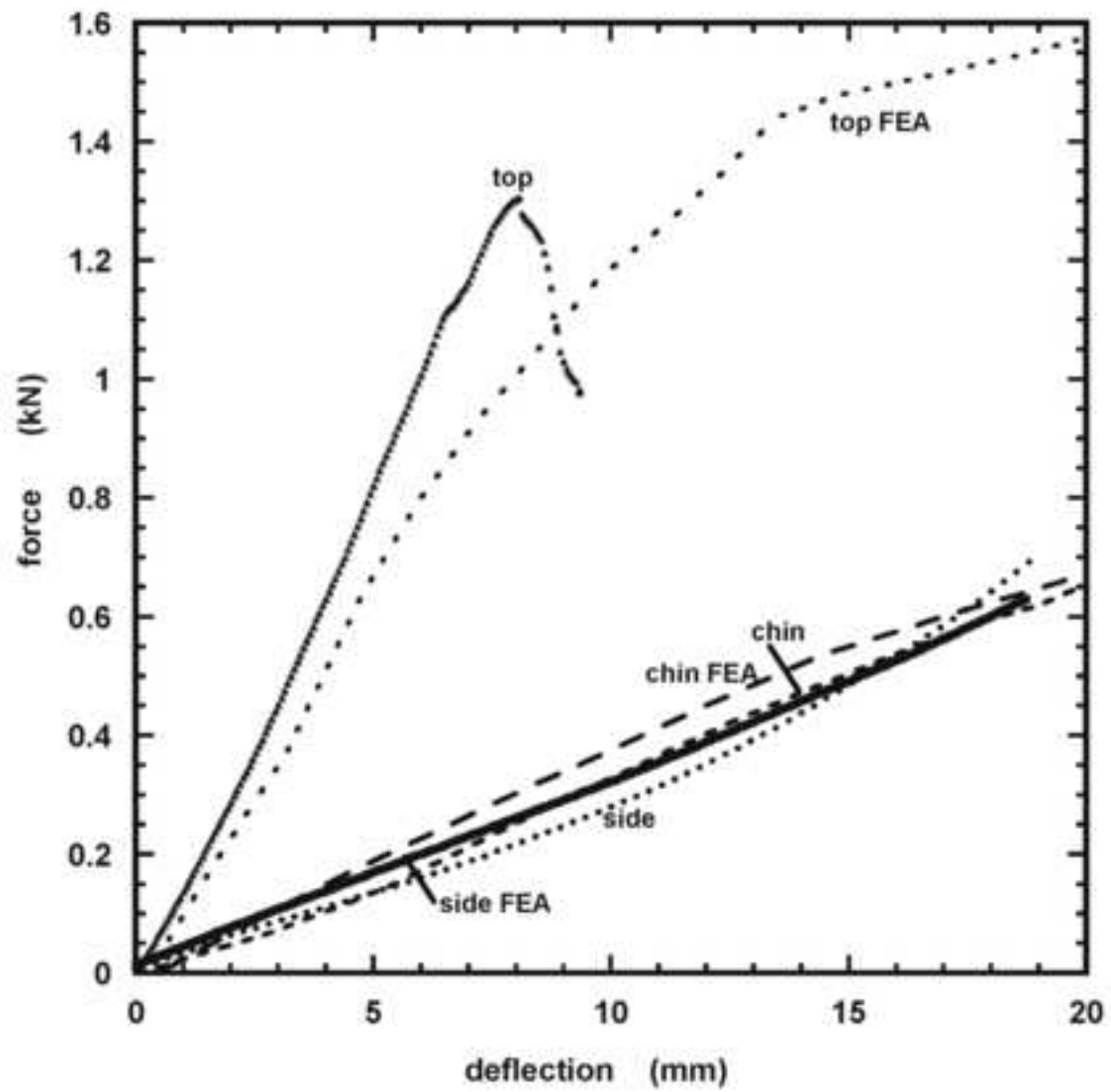
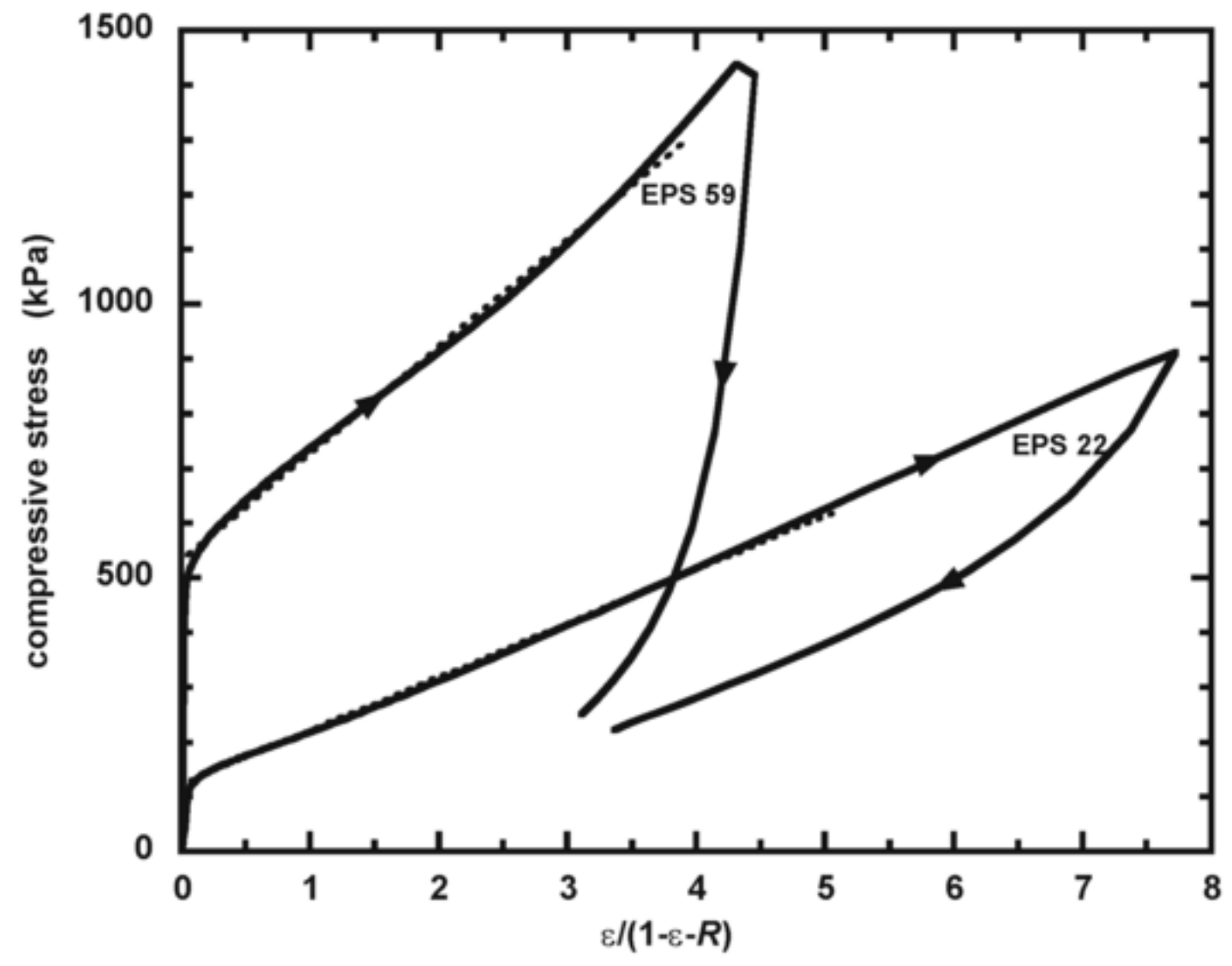
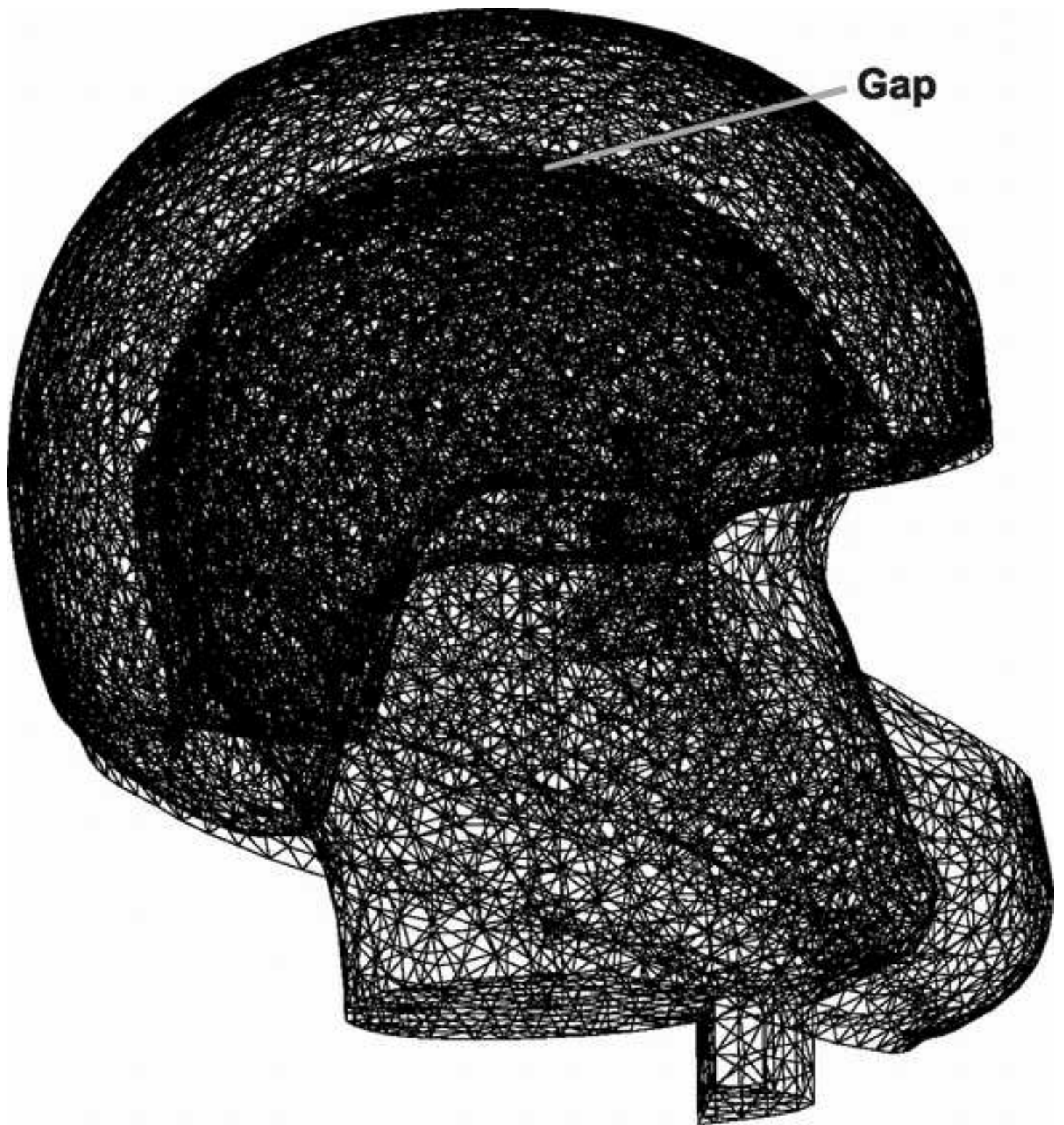
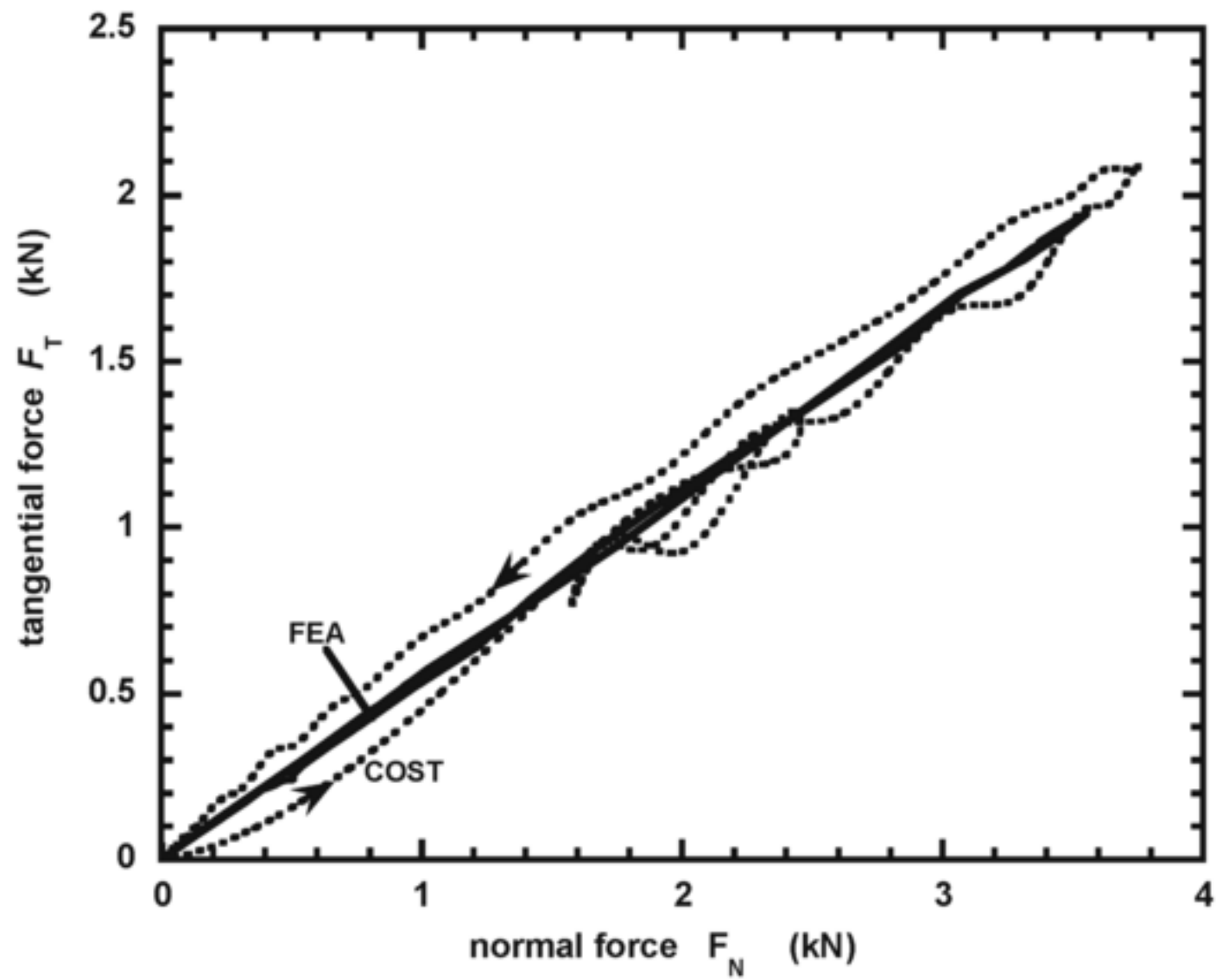
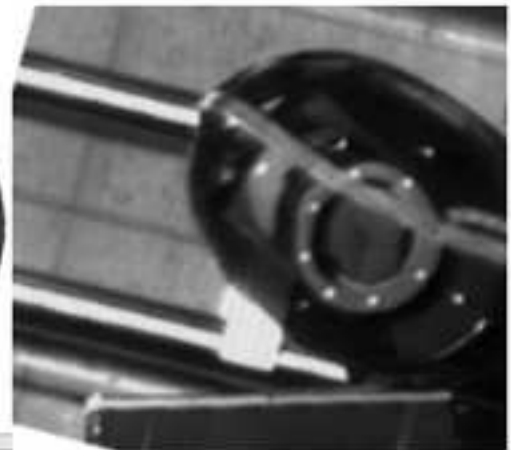
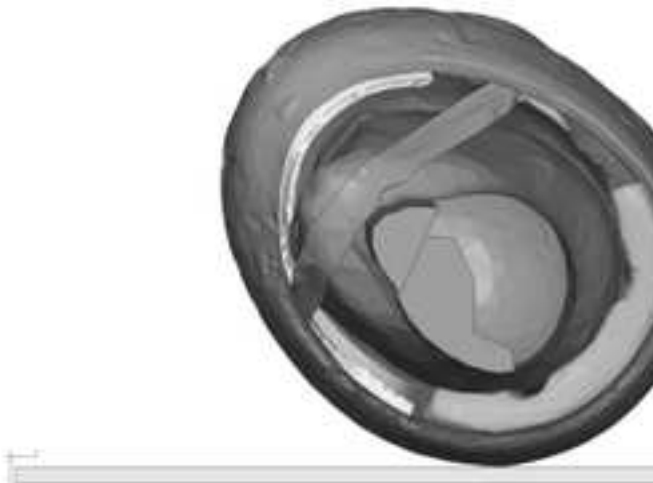
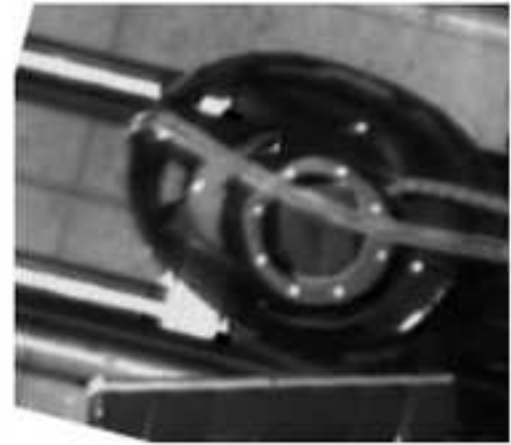
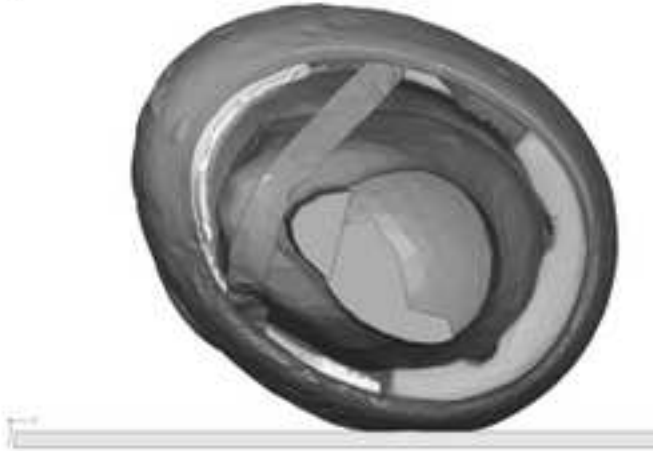
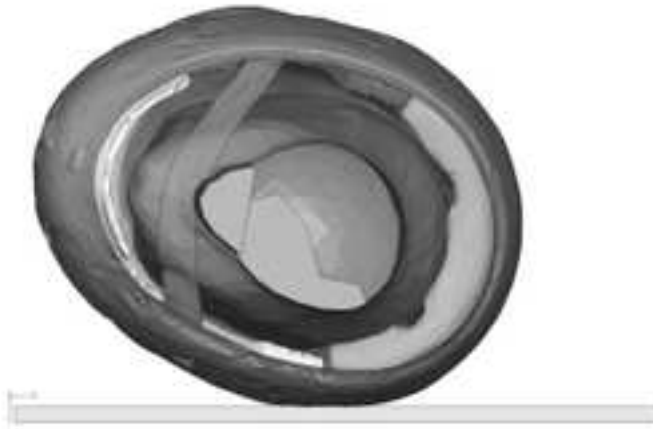


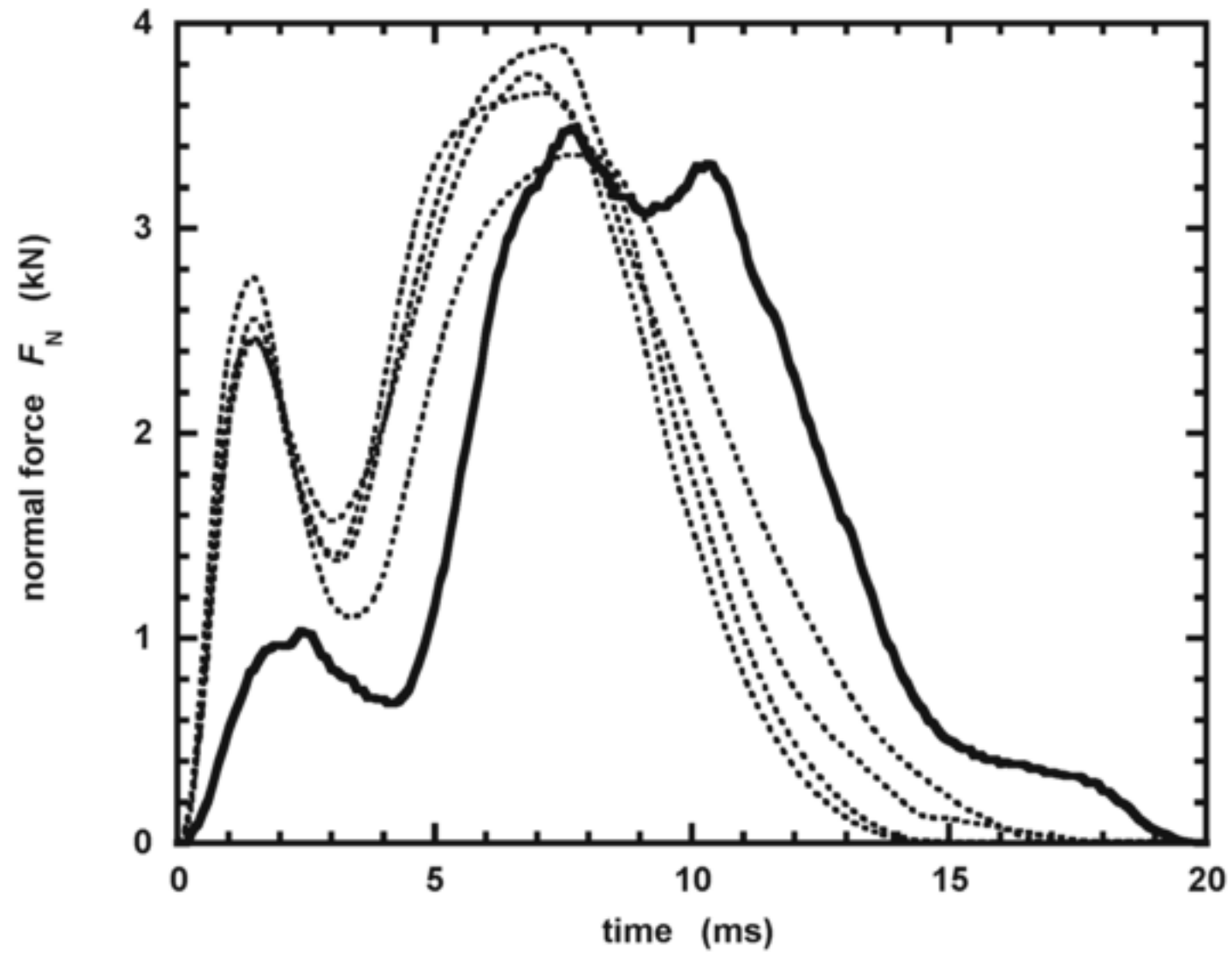
Figure 6

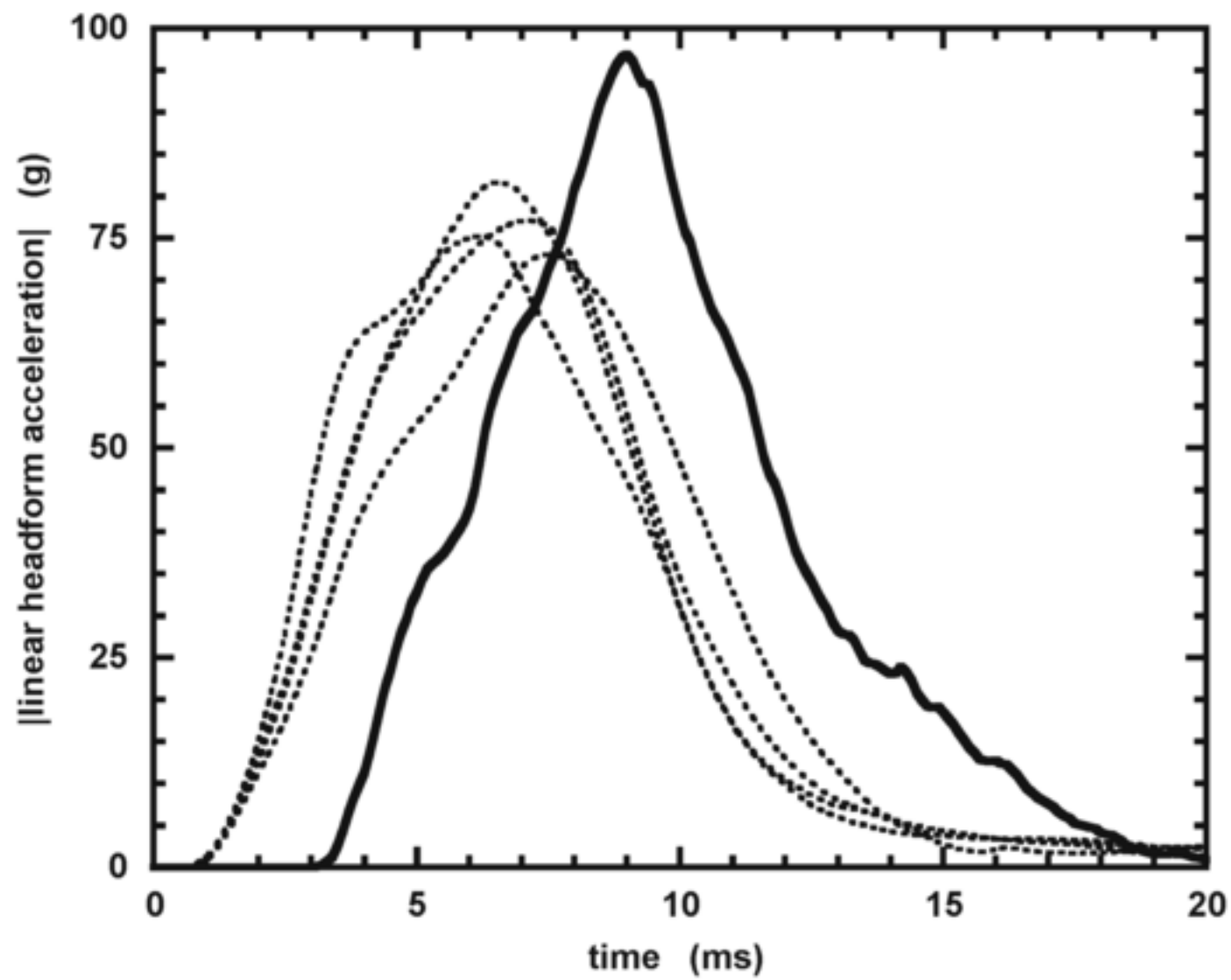


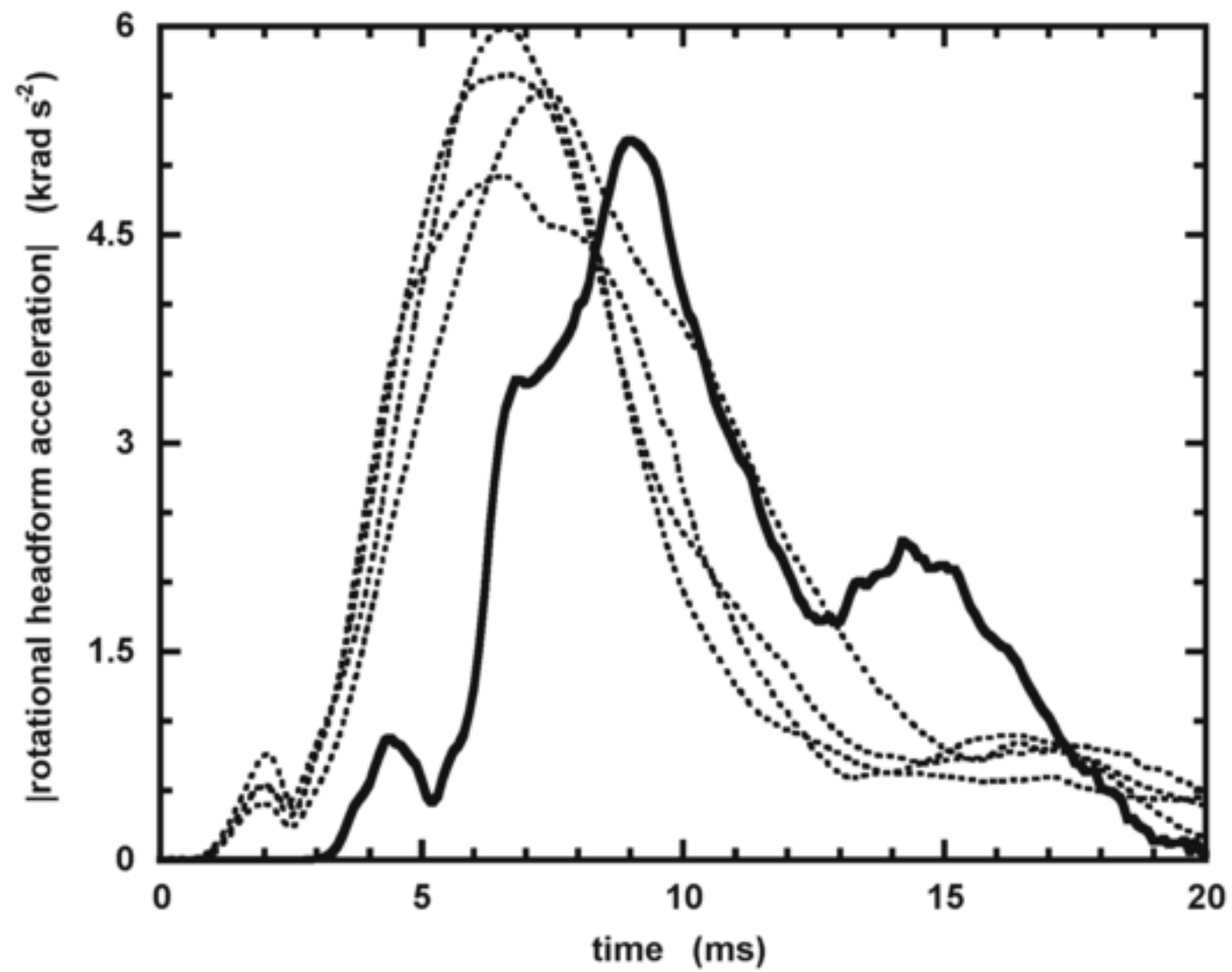


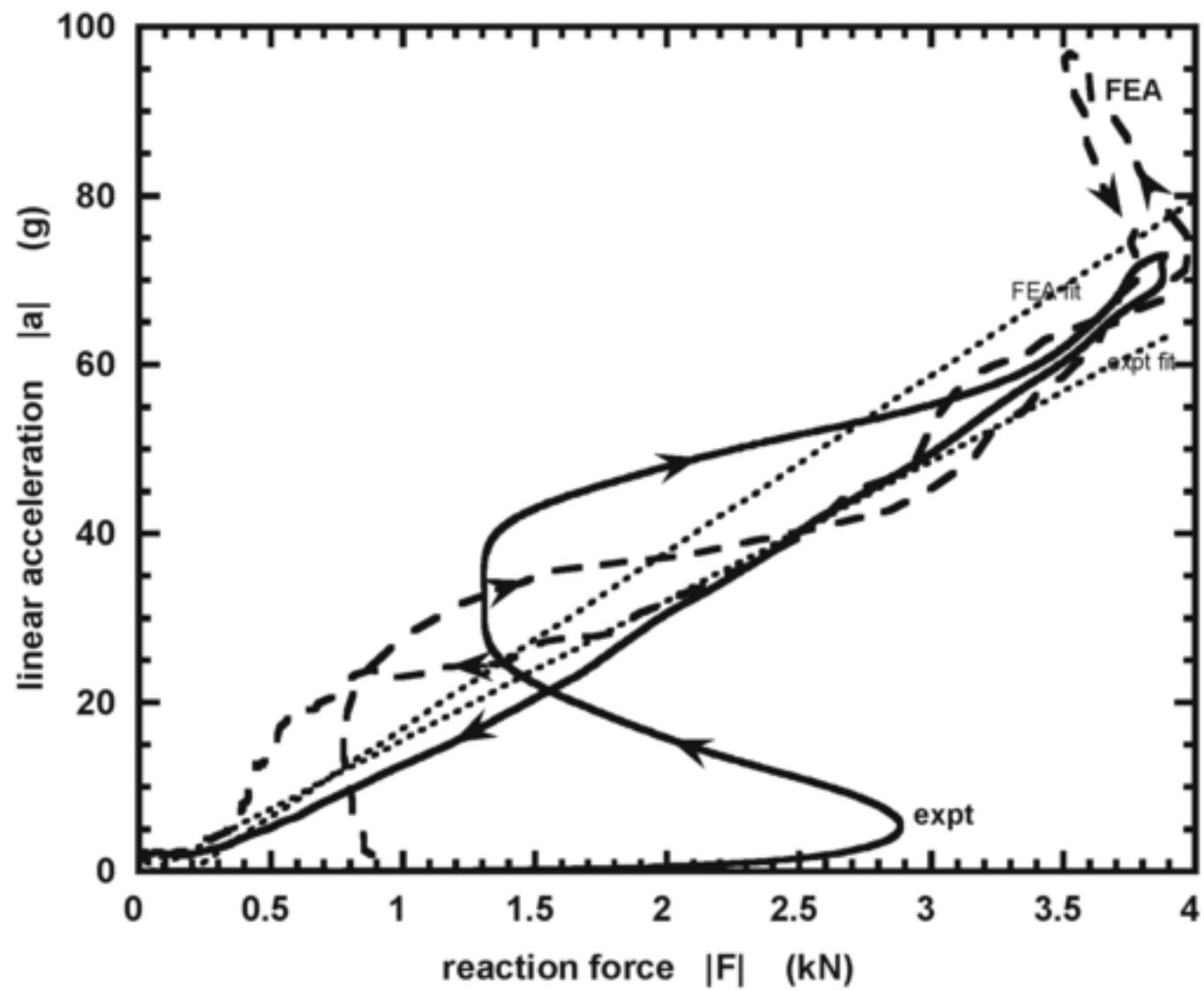


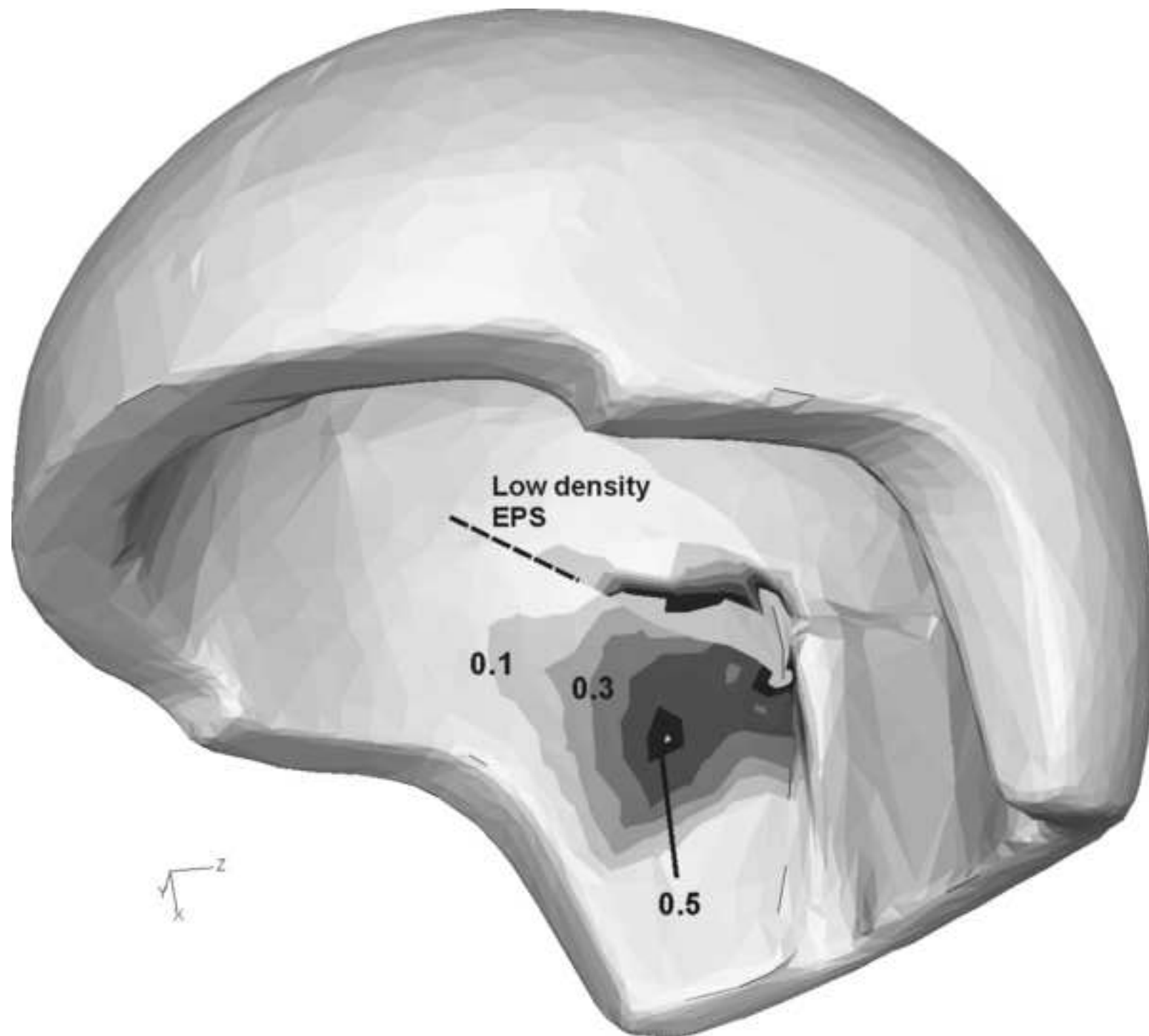


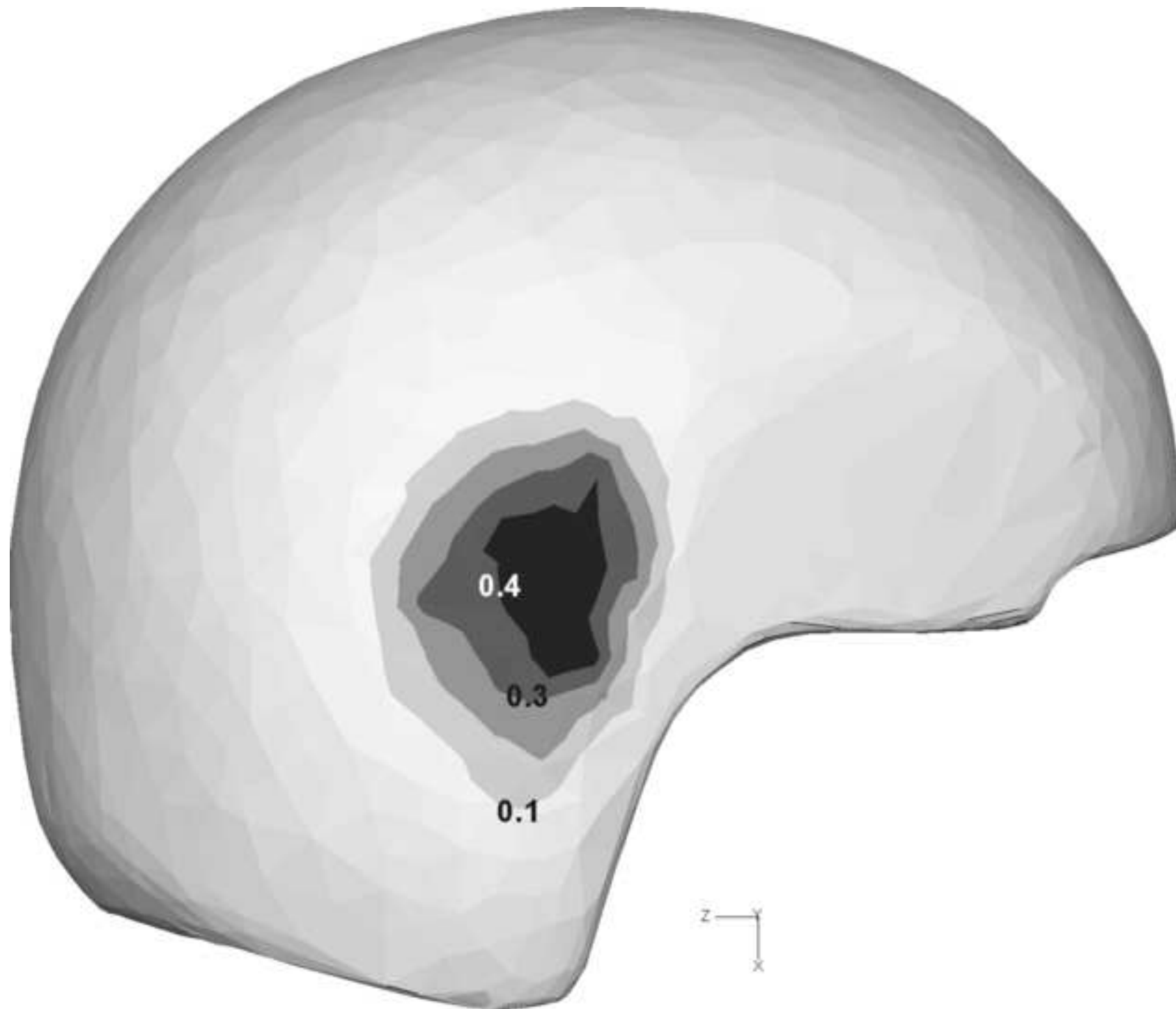


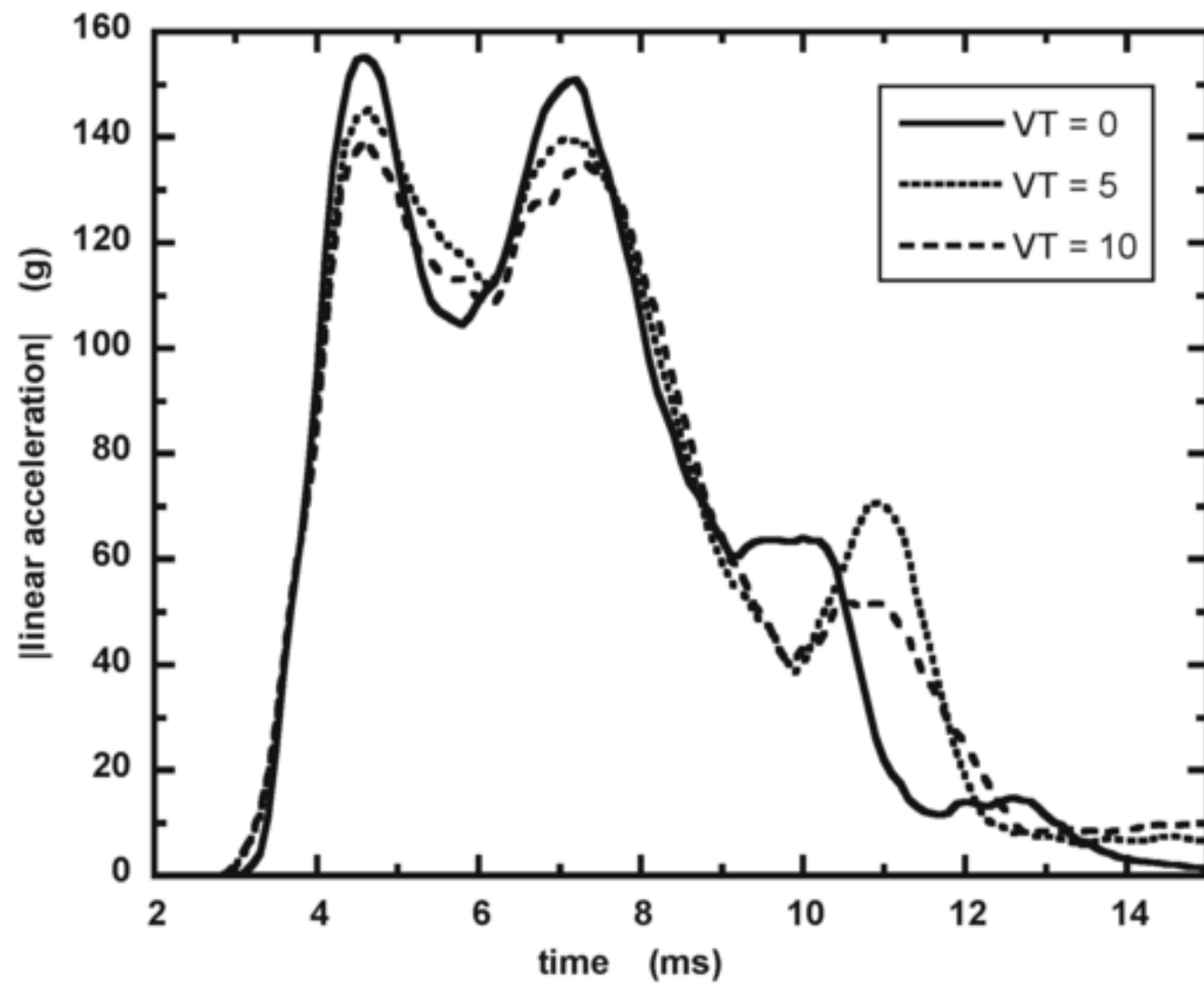


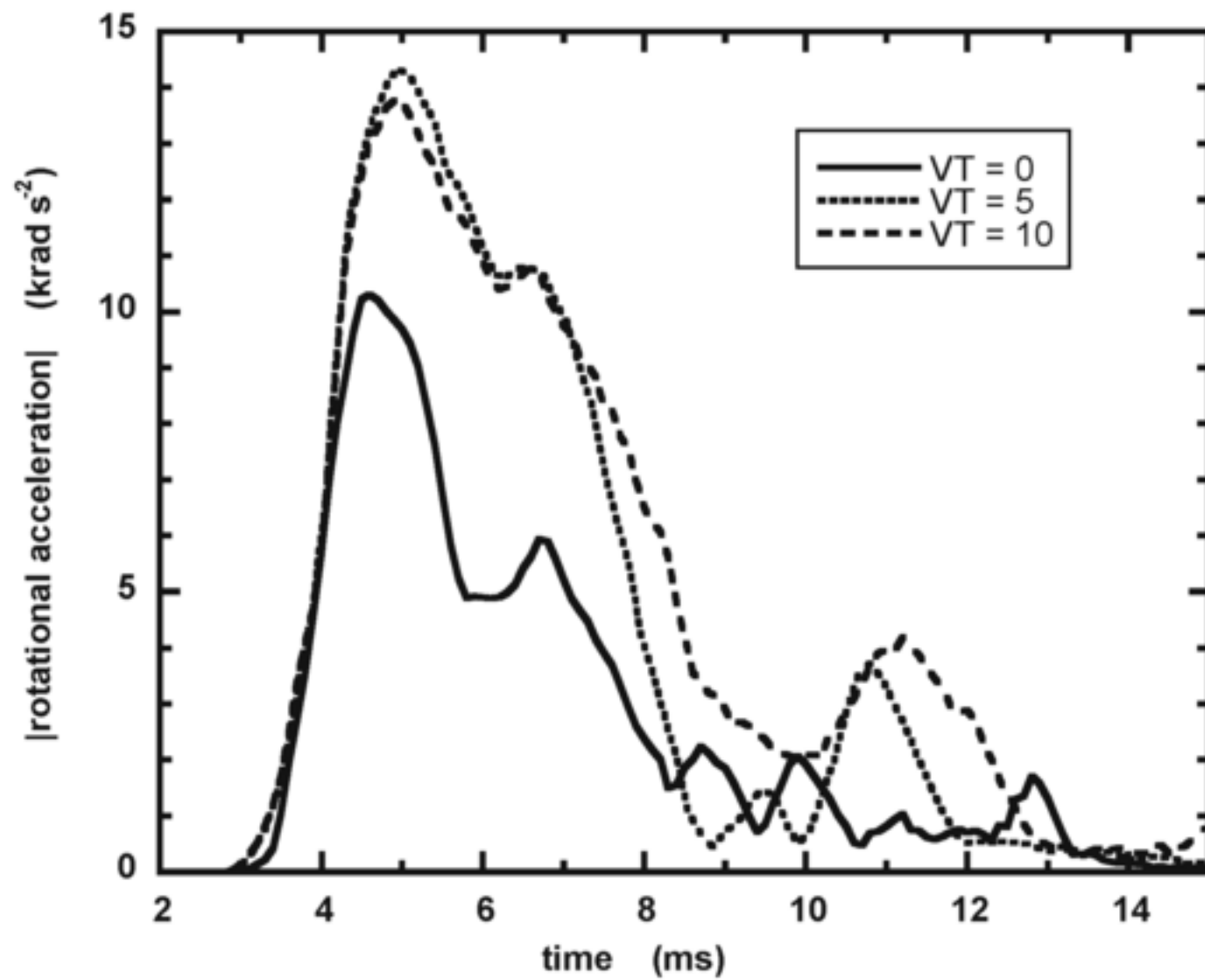












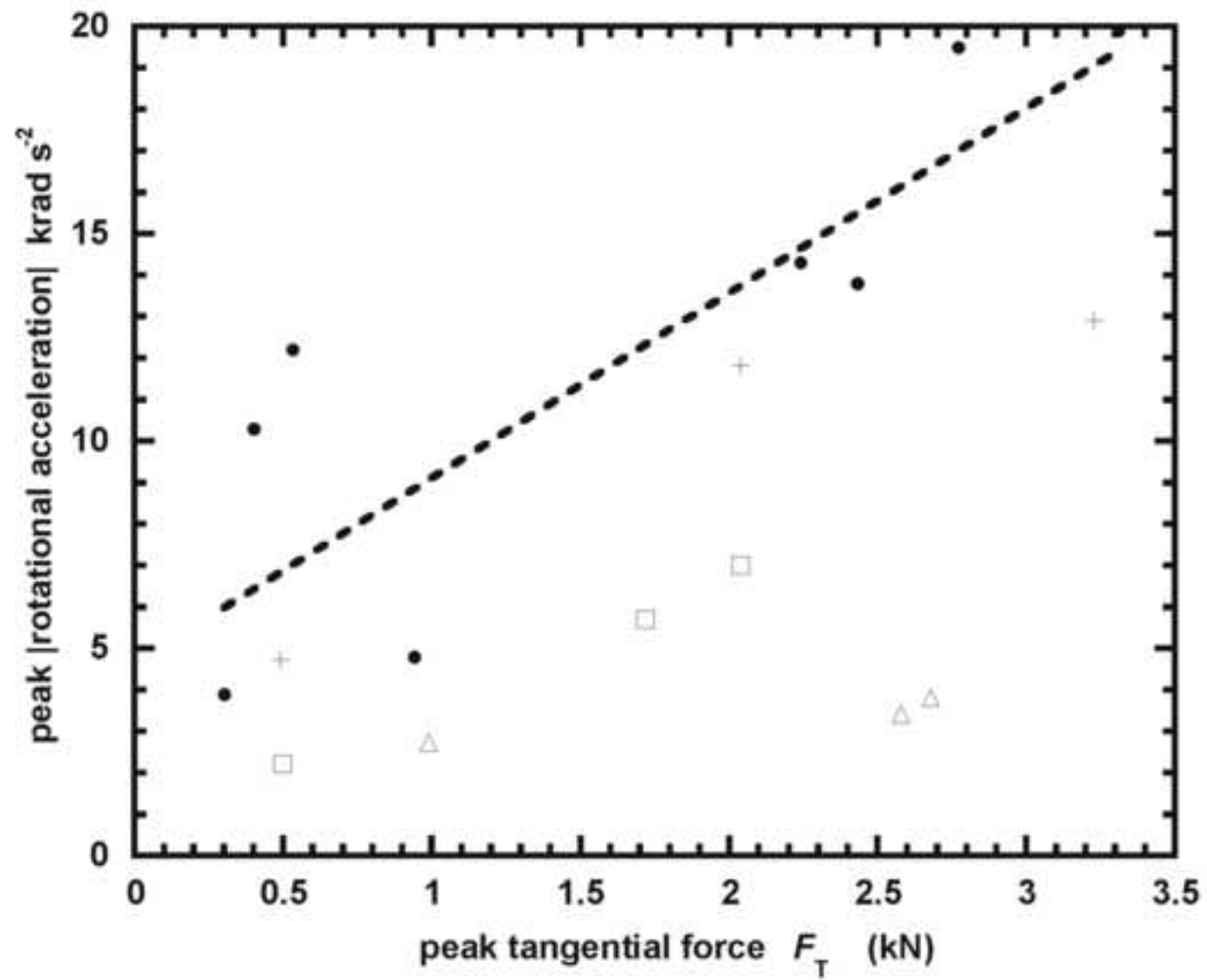


Figure 15

